

MAGNETIC NANOPARTICLES STABILIZED BY PHOSPHORYLCHOLINE-CONTAINING
POLYMER FOR ANTIBODY FREE C-REACTIVE PROTEIN DETECTION



A Thesis Submitted in Partial Fulfillment of the Requirements
for the Degree of Master of Science in Petrochemistry and Polymer Science
Field of Study of Petrochemistry and Polymer Science
FACULTY OF SCIENCE
Chulalongkorn University
Academic Year 2019
Copyright of Chulalongkorn University

อนุภาคนาโนแม่เหล็กซึ่งทำให้เสถียรด้วยพอลิเมอร์ที่มีฟอสโฟริลโคลีนสำหรับการตรวจวัดซี-รีแอกทีฟ
โปรตีนแบบปราศจากแอนติบอดี



วิทยานิพนธ์นี้เป็นส่วนหนึ่งของการศึกษาตามหลักสูตรปริญญาวิทยาศาสตรมหาบัณฑิต
สาขาวิชาปิโตรเคมีและวิทยาศาสตร์พอลิเมอร์ สาขาวิชาปิโตรเคมีและวิทยาศาสตร์พอลิเมอร์
คณะวิทยาศาสตร์ จุฬาลงกรณ์มหาวิทยาลัย
ปีการศึกษา 2562
ลิขสิทธิ์ของจุฬาลงกรณ์มหาวิทยาลัย

6072185023 : MAJOR PETROCHEMISTRY AND POLYMER SCIENCE

KEYWORD: C-reactive protein, poly[methacrylic acid)-*ran*-(methacryloyloxyethyl phosphorylcholine)], phosphorylcholine, MNPs

Suttawan Saipia : MAGNETIC NANOPARTICLES STABILIZED BY PHOSPHORYLCHOLINE-CONTAINING POLYMER FOR ANTIBODY FREE C-REACTIVE PROTEIN DETECTION. Advisor: Assoc. Prof. VORAVEE HOVEN, Ph.D.

This research aims to develop a simple, yet effective assay for C-reactive protein (CRP) detection based on a combination of magnetic separation and antibody-free colorimetric assay. Magnetic nanoparticles stabilized with phosphorylcholine-containing polymer, poly[methacrylic acid)-*ran*-(methacryloyloxyethyl phosphorylcholine)] (PMAMPC-MNPs) were prepared by coprecipitation of ferric and ferrous salts in the presence of PMAMPC. Carboxyl groups in the methacrylic acid (MA) repeat units chelate with Fe atoms during MNPs formation while the methacryloyloxyethyl phosphorylcholine (MPC) repeat units provide specifically binding sites and conjugate with CRP in presence of Ca^{2+} . The PMAMPC-MNPs were characterized by ATR-FTIR, TEM, DLS, TGA and XRD. To determine the CRP binding, the PMAMPC-MNPs were mixed with CRP in presence of Ca^{2+} and then precipitation of PMAMPC-MNPs conjugated with CRP was induced by magnet. Taking advantage of peroxidase-like activity of MNPs, an addition of 3,3',5,5'-tetramethylbenzidine (TMB) and H_2O_2 in 0.1 M acetate buffer, pH 3.8 to the supernatant allows colorimetric determination for a short period of time of unbound PMAMPC-MNPs which is inversely proportional to the amount of CRP and detects in antibody-free system. A linear range of 0 – 5 $\mu\text{g}/\text{ml}$ and detection limit of 1.39 $\mu\text{g}/\text{mL}$. Moreover, 3 $\mu\text{g}/\text{ml}$ CRP in undiluted rabbit serum can be detected as well.

Field of Study: Petrochemistry and Polymer Science Student's Signature

Academic Year: 2019 Advisor's Signature

ACKNOWLEDGEMENTS

First of all, I would like to express my sincere gratitude to my advisor, Associate Professor Dr. Voravee Hoven for her generous advice, invaluable guidance and encouragement throughout the course of this research. Working with her has been the best course of my study.

I sincerely thank to Assistant Professor Dr. Warinthorn Chavasiri, Associate Professor Dr. Vimolvann Pimphan and Dr. Piyaporn Na Nongkhai. For acting as the chairman and examiner of my thesis committee, respectively and for their valuable constructive comments and suggestions.

Financial support for this work was provided by Chulalongkorn University (CU_GR_62_93_23_34) and the National Nanotechnology Center (NANOTEC), NSTDA, Ministry of Science and Technology, Thailand, through its program of Research Network NANOTEC (RNN) and Department of Chemistry, Faculty of Science, Center of Excellence for Innovation in Chemistry and Sensor Research Unit, Burapha University.

Furthermore, I would like to thank members of VH's group for providing the chemicals, facilities throughout the course of study, their friendliness, helpful discussion and encouragements.

Finally, I would like to express my thankfulness to my beloved parent who always stand by my side during pleasant and difficult times.

Suttawan Saipia

TABLE OF CONTENTS

	Page
ABSTRACT (THAI).....	iii
ABSTRACT (ENGLISH).....	iv
ACKNOWLEDGEMENTS.....	v
TABLE OF CONTENTS.....	vi
LIST OF FIGURES.....	viii
LIST OF TABLES.....	xi
LIST OF ABBREVIATION.....	xii
CHAPTER I INTRODUCTION.....	1
1.1 Introduction.....	1
1.2 Objectives.....	13
1.3 Scope of investigation.....	13
CHAPTER II EXPERIMENTAL.....	14
2.1 Materials.....	14
2.2 Equipments.....	14
2.2.1. Attenuated Total Reflectance-Fourier Transform Infrared Spectroscopy (ATR-FTIR).....	14
2.2.2. Thermogravimetric Analysis (TGA).....	15
2.2.3. Transmission Electron Microscopy (TEM).....	15
2.2.4. X-ray Diffraction (XRD).....	15
2.2.5. Dynamic Light Scattering (DLS).....	15
2.2.6. UV-Vis Spectroscopy (UV-Vis).....	16

2.2.7. Nuclear Magnetic Resonance Spectroscopy (NMR)	16
2.3 Experimental Procedure	16
2.3.1. Synthesis of PMAMPC by RAFT polymerization	16
2.3.2. Preparation of PMAMPC-functionalized MNPs by two-step co-precipitation.....	17
2.3.3. Colloidal stability of PMAMPC-MNPs	18
2.3.4. Conjugation of PMAMPC-MNPs with CRP	18
2.3.5. Colorimetric detection of CRP using PMAMPC-MNPs with TMB/H ₂ O ₂	19
CHAPTER III	21
RESULTS AND DISCUSSION.....	21
3.1 Preparation and Characterization of PMAMPC-MNPs	21
3.2 Conjugation of PMAMPC-MNPs with CRP	27
3.3 Colorimetric detection of CRP using PMAMPC-MNPs with TMB/H ₂ O ₂	33
CHAPTER IV	39
CONCLUSION AND SUGGESTIONS.....	39
REFERENCES	41
VITA.....	48

LIST OF FIGURES

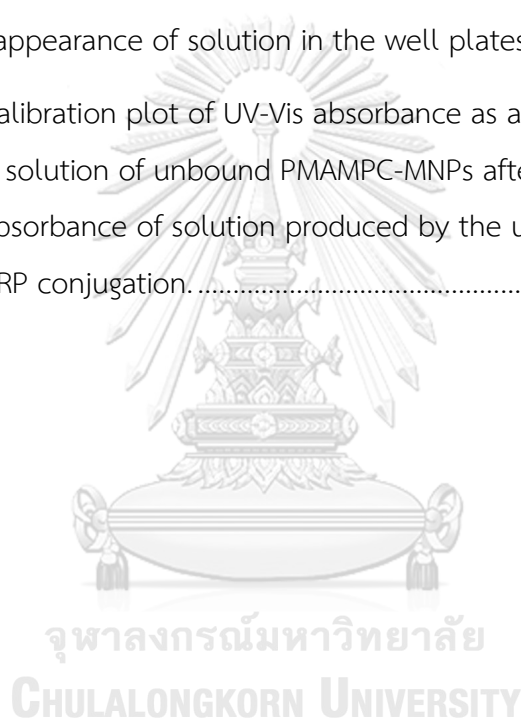
	Page
Figure 1.1 Stabilization of CRP with 1,6-bis PC abolished nCRP formation and deposition <i>in vivo</i>	2
Figure 1.2 (a) Chemical structure of PMBN polymer and (b) FE-SEM micrograph of MPC-PNP prepared by solvent evaporation technique.....	3
Figure 1.3 (a) Preparation of AuNPs surface-modified with thiol-terminated PMPC- <i>b</i> -PMAT and (b) appearance of AuNPs solution in the presence of CRP having varied concentration.	4
Figure 1.4 Magnetic-based sandwich hybridization assay for CRP detection using quantum dot fluorescence labeling and immunoaffinity separation.....	5
Figure 1.5 Immunomagnetic sandwich hybridization assay using anti-CRP-labeled fluorescent nanoparticles for CRP detection.....	6
Figure 1.6 Preparation of PC-functionalized MNPs for CRP isolation.	7
Figure 1.7 (a) Preparation of poly(MPC)-stabilized Fe ₃ O ₄ nanoparticles by hydrothermal treatment and SI-ATRP of MPC. (b) Change in the size of poly(MPC)-stabilized Fe ₃ O ₄ nanoparticles in contact with CRP aggregation of poly(MPC)-stabilized Fe ₃ O ₄ nanoparticles with CRP without (blue circles) and with using a neodymium magnet in buffer (red circles) in 0.35 g/dL albumin (black triangles) and (c) TEM images of poly(MPC)-protected Fe ₃ O ₄ nanoparticles before and after contacting with 100 nM CRP for 60 min.....	8
Figure 1.8 Catalytic oxidation by MNPs of TMB which acts as a hydrogen donor for the reduction of H ₂ O ₂ reduction. The resulting diimine leads to the blue solution. ⁴³	9
Figure 1.9 Colorimetric glucose detection by using GOx in combination with H ₂ TCPP-Fe ₃ O ₄	10
Figure 1.10 MNP-based colorimetric detection of <i>S. typhimurium</i> using label-free DNA aptamers and TMB.	11

Figure 1.11 (A) Preparation of Fe ₃ O ₄ NPC, (B) detection of <i>L. Monocytogenes</i> using aptamer-modified Fe ₃ O ₄ NPC, and (C) Signal amplification using TMB/H ₂ O ₂ as chromogenic substrate catalyzed by the Fe ₃ O ₄ NPC.....	12
Figure 2.1 Synthesis of PMAMPC by RAFT polymerization.....	17
Figure 2.2 Preparation of PMAMPC-functionalized MNPs by two-step co-precipitation.....	18
Figure 2.3 Detection of CRP using PMAMPC-MNPs with TMB/H ₂ O ₂	20
Figure 3.1 ¹ H-NMR spectra of (i) crude and (ii) purified PMAMPC.....	23
Figure 3.2 ATR-IR spectra of (a) bare MNPs, PMAPMC-MNPs prepared by using PMAMPC of (b) 10, (c) 40, (d) 100, and (e) 150 mg and (f) PMAMPC.....	24
Figure 3.3 Appearance of aqueous dispersion of bared MNPs and PMAMPC-MNPs prepared using varied PMAMPC quantity as a function of time.....	25
Figure 3.4 XRD spectra of (a) bare MNPs, PMAPMC-MNPs prepared by using PMAMPC of (b) 10, (c) 40, (d) 100, and (e) 150 mg.....	26
Figure 3.5 TGA (under N ₂) curves of (a) bare MNPs, PMAPMC-MNPs prepared by using PMAMPC of (b) 10, (c) 40, (d) 100, and (e) 150 mg with a heating rate of 20°C/min. ..	27
Figure 3.6 Appearance of colloidal PMAMPC-MNPs (0.4 mg/mL) in the presence of varied CaCl ₂ concentration as a function of incubation time.....	28
Figure 3.7 Appearance of colloidal PMAMPC-MNPs of varied concentration before and after the addition of CRP (20 µg/mL) in the presence of 1 mM Ca ²⁺ as a function of incubation time.....	29
Figure 3.8 Appearance of colloidal PMAMPC-MNPs upon an addition of (a) varied CRP concentration as a function of time, (B) CRP in comparison with HSA and γ -globulin, (C) Ca ²⁺ and Ca ²⁺ together with CRP under the external magnetic field.....	30
Figure 3.9 (a) DLS profiles and (b) zeta potential values of bare MNPs and PMAMPC-MNPs both before and after the addition of CRP (5 µg/mL) in the presence of 1 mM Ca ²⁺	31

Figure 3.10 TEM micrographs of (a) bare MNPs, PMAPMC-MNPs both (b) before and (c) after conjugation with CRP (5 $\mu\text{g/mL}$) in the presence of 1 mM Ca^{2+} . (scale bar = 100 nm (left) and 50 nm (right)). 32

Figure 3.11 UV-Vis absorption (a) spectra and (b) bar graphs of UV-Vis absorbance at 650 nm of PMAMPC-MNPs + TMB + H_2O_2 (black solid line and black filled strip), PMAMPC-MNPs + TMB (black dashed line and black pattern), PMAMPC-MNPs + H_2O_2 (red dashed line and red pattern), TMB + H_2O_2 (blue dashed line and blue pattern), and PMAMPC-MNPs + CRP + TMB + H_2O_2 (red solid line and red filled strip). The insets in (b) show appearance of solution in the well plates..... 34

Figure 3.12 (a) A calibration plot of UV-Vis absorbance as a function of CRP concentration and solution of unbound PMAMPC-MNPs after oxidation with TMB and H_2O_2 . (b) UV-Vis absorbance of solution produced by the unbound PMAMPC-MNPs before and after CRP conjugation..... 36



LIST OF TABLES

Page

Table 3.1 Analytical characteristics for different CRP biosensors reported.....	38
--	----



LIST OF ABBREVIATION

ACVA	: 4,4-Azobis(4-cyanovaleric acid)
ATR - FTIR	: Attenuated total reflectance-Fourier transform infrared spectroscopy
CPD	: 4-Cyano-4-(phenylcarbonothio) pentanoic acid
CRP	: C-reactive protein
DW	: Deionized water
DLS	: Dynamic light scattering
HSA	: Human serum albumin
LOD	: Limit of detection
MNPs	: Magnetic nanoparticles
NMR	: Nuclear magnetic resonance spectrometer
PMAMPC	: Poly[methacrylic acid)- <i>ran</i> - (methacryloyloxyethyl phosphorylcholine)]
RAFT	: Reversible addition-fragmentation chain transfer
TEM	: Transmission electron microscopy
TGA	: Thermogravimetric analysis
TMB	: 3,3',5,5'-Tetramethylbenzidine
UV-Vis	: UV-Vis spectrophotometer
XRD	: X-ray diffraction

CHAPTER I

INTRODUCTION

1.1 Introduction

Cardiovascular disease is the top cause of death for Thai people. Especially in the elderly people who are at greater risk of developing the disease than other age groups. The risk of cardiovascular diseases can be assessed by measuring the number of biomarkers in the blood such as homocysteine, cholesterol and C-reactive protein (CRP).¹ The native CRP (nCRP) is pentameric protein of which each subunit has a phosphocholine (PC) binding site and two calcium ions (Ca^{2+}) per protomer as shown in **Figure 1.1**. Each subunit has a 23 kDa molecular mass and 206 amino acids.² The calcium ions are important for the stability and binding of ligands.²⁻⁴ The CRP is generated by the liver in response to tissue injury and inflammation. Its level in blood can therefore be used to assess the severity of inflammation and to be a risk factor for certain diseases, especially cardiovascular disease. Inflammation caused by cardiovascular disease can occur within the arteries. After the epithelial cells of the arteries are destroyed and repaired, swelling and redness are a part of the inflammation. Then, there is an accumulation of cholesterol when there is chronic inflammation of the blood vessels that thickens the vascular wall. The American Heart Association recommends that a blood CRP test may be used as a means of assessing cardiovascular risk and people having high cardiovascular risk that have CRP in the blood is more than 3.0 mg/L.^{5, 6} Currently, CRP assays can be performed in a laboratory using a variety of methods, including nephelometry,^{7, 8} immunoturbidimetry^{9, 10} and enzyme-linked immunosorbent assay (ELISA)¹¹ etc. These methods are highly effective but there are limitations on analysis time, costly,

inability to perform out-of-laboratory experiments and require the expertise for analysis.

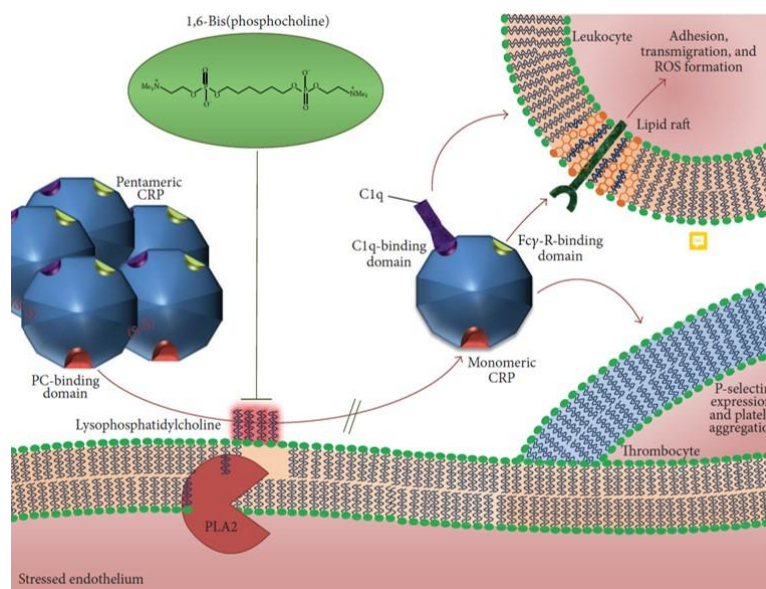


Figure 1.1 Stabilization of CRP with 1,6-bis PC abolished nCRP formation and deposition *in vivo*.⁴

2-Methacryloyloxyethyl phosphorylcholine (MPC) based polymers have been widely employed in gene/drug delivery systems due to their excellent biocompatibility, and recognized as an artificial cell membrane.¹²⁻¹⁴ MPC with cell-membrane mimic structure is utilized as a polymerizable specific ligand toward CRP. Poly(MPC) (PMPC) is one of well-known zwitterionic polymer that can effectively suppress nonspecific adsorption of other proteins in the presence with CRP. PMPC should thus be a potential and efficient artificial probe for selective CRP sensing.¹⁵⁻¹⁷

A number of research work have been reported on detection of CRP using MPC-based polymers:

In 2004, Park *et al.*¹⁸ prepared polymeric nanoparticles from poly[MPC-co-*n*-butyl methacrylate (BMA)-co-*p*-nitrophenyloxycarbonyl poly(ethylene glycol)

methacrylate (PMBN) as shown in **Figure 1.2**. By using solvent evaporation, the MPC-polymeric nanoparticles (MPC-PNP) were prepared by using poly(L-lactic acid) as a core and PMBN as an surface modifier and emulsifier. The MPC-PNP having active ester groups were conjugated with monoclonal antibody CRP followed by blocking the remaining active ester groups by reacting with glycine, the resulting antibody CRP-conjugated MPC-PNP were used to detect CRP by immunoagglutination assay in comparison with polystyrene nanoparticles. A linear range of CRP detection was found to be 0.01-10 and 0.1-10 mg/dL for serum-free solution and serum, respectively.

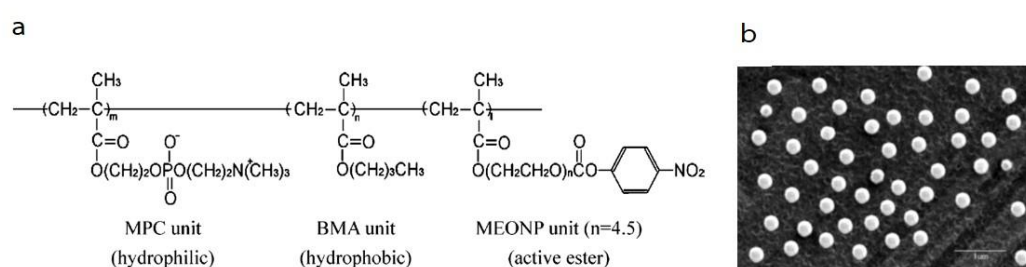


Figure 1.2 (a) Chemical structure of PMBN polymer and (b) FE-SEM micrograph of MPC-PNP prepared by solvent evaporation technique.¹⁸

In 2014, Iwasaki *et al.*¹⁹ synthesized AuNPs modified with thiol-terminated block copolymer of poly(2-methacryloyloxyethyl phosphorylcholine)-*b*-poly(N-methacryloyl-(L)-tyrosine methylester) (PMPC-*b*-PMAT) (**Figure 1.3a**). The AuNPs surface-modified with PMPC-*b*-PMAT exhibited good colloidal stability due to steric stabilization of hydration layer of the copolymer. Aggregation of the particles as a result of inter-particle crosslinking was induced in the presence of Ca^{2+} and CRP in a concentration range of about 0 – 100 nM. A detection limit was between 20 and 40 nM. (**Figure 1.3b**).

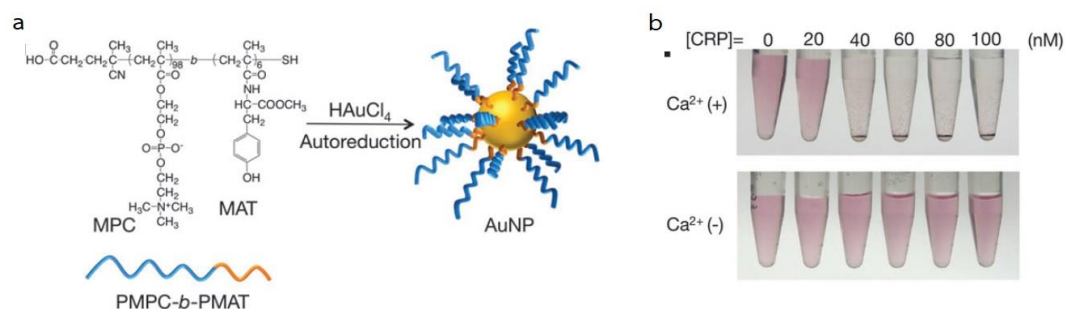


Figure 1.3 (a) Preparation of AuNPs surface-modified with thiol-terminated PMPC-*b*-PMAT and (b) appearance of AuNPs solution in the presence of CRP having varied concentration.¹⁹

In 2019, Pinyorospatum *et al.*²⁰ developed a paper-based electrochemical sensor. AuNPs electrodeposited on screen-printed electrode (SPE) were modified by self-assembly of thiol-terminated PMPC. The SPE sensor can detect CRP in the presence of Ca^{2+} by differential pulse voltammetry (DPV) to give high sensitivity and low limit of detection. The current of DPV is low at high CRP concentration. Moreover, this assay as an antibody-free CRP sensor can detect CRP in a concentration range of 5-5,000 ng/mL and a detection limit of 1.55 ng/mL.

Magnetic nanoparticles (MNPs) have been widely recognized as their potential for biomagnetic separation and detection. MNPs are usually in magnetite form (Fe_3O_4) and have size in range of 5-500 nm which can be attracted to magnet²¹. From aforementioned properties, Fe_3O_4 exhibit a great potential especially for the rapid magnetic separation of protein, bacteria and biomolecules due to their response to magnetic field and large surface to volume ratio that can induce an efficient interaction with the target analytes even in a dilute sample containing various background materials.²²⁻²⁴

A number of research work has been reported on biomagnetic separation and detection:

In 2010, Zhu *et al.*²³ developed magnetic-based sandwich hybridization assay for CRP detection. Micro magnetic beads immobilized with monoclonal anti-CRP were first used to capture CRP followed by incubation with biotinylated monoclonal anti-CRP and Streptavidin-coated quantum-dot (QDs). The sandwich-hybridized immunocomplexes were subjected to immunoaffinity separation and magnetic separation. The amount of CRP was then quantified from fluorescence signal of released QDs (**Figure 1.4**). A detection limit of 0.5 fM which corresponds to 10 pM CRP in 50 μ L of sample volume.

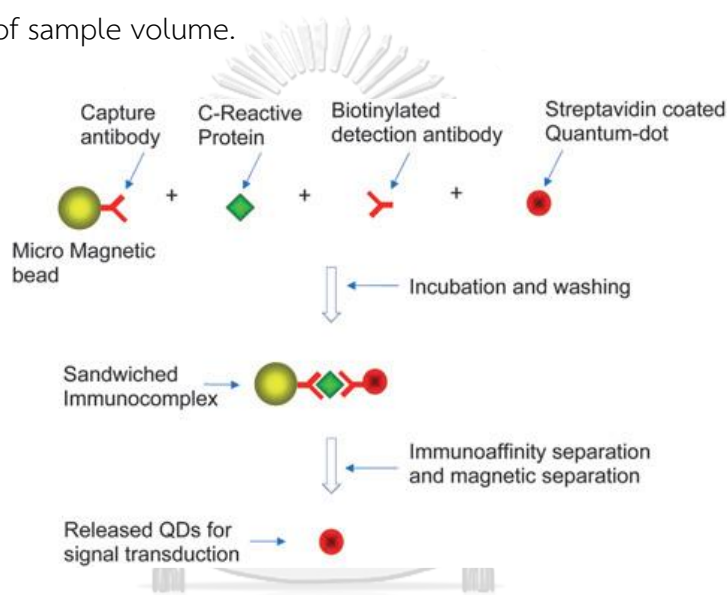


Figure 1.4 Magnetic-based sandwich hybridization assay for CRP detection using quantum dot fluorescence labeling and immunoaffinity separation.²³

In 2014, Yang *et al.*²⁴ developed magnetic immunoassay for CRP detection. Silica-modified magnetic nanoparticles were first prepared and conjugated with monoclonal anti-CRP to yield anti-CRP-labeled magnetic particles. The particles were used to capture CRP. The detection was done by using anti-CRP-labeled fluorescent nanoparticles (**Figure 1.5**). The fluorescence intensity of this assay was detected and relate with CRP concentration. A linear range of 1.18 - 11.8 μ g/mL and a limit of detection of 1.0 ng/mL were reported.

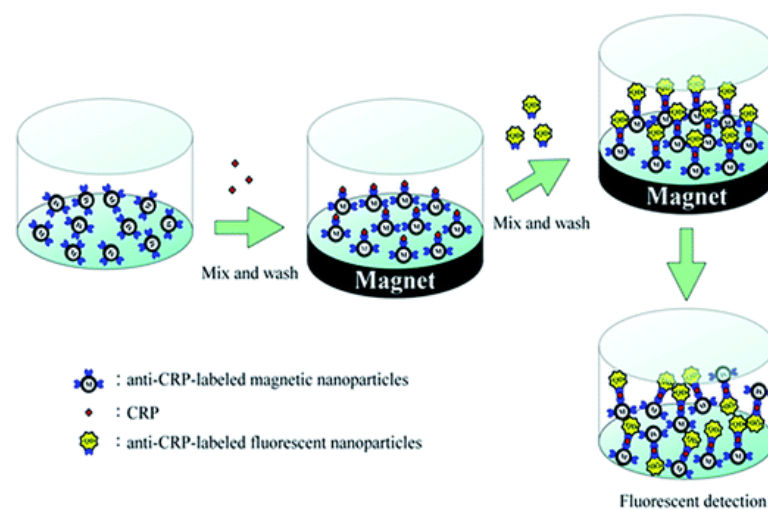


Figure 1.5 Immunomagnetic sandwich hybridization assay using anti-CRP-labeled fluorescent nanoparticles for CRP detection.²⁴

A number of research work have been reported on stabilization of MNPs with copolymer having phosphorylcholine (PC) groups for CRP measurement.

In 2013, Kim *et al.*²⁵ developed PC-functionalized MNPs for rapid and efficient CRP isolation. Methacrylate-modified MNPs were first prepared by reacting oleic acid-coated MNPs with 3-methacryloxypropyltrimethoxysilane (MPS). 3-(4-vinylbenzyl)-12-phosphorylcholine dodecanoate (VPC) was then polymerized on the MPS-modified MNPs and yielded VPC-MNPs (**Figure 1.6**). CRP in human serum solution was captured by VPC-MNPs. CRP was released by using elution buffer. CRP-binding capacity of VPC-MNPs was higher than that of the as determined by ELISA. The CRP fraction was characterized by sodium dodecylsulfate-polyacrylamide gel and confirmed by peptide mass fingerprinting.

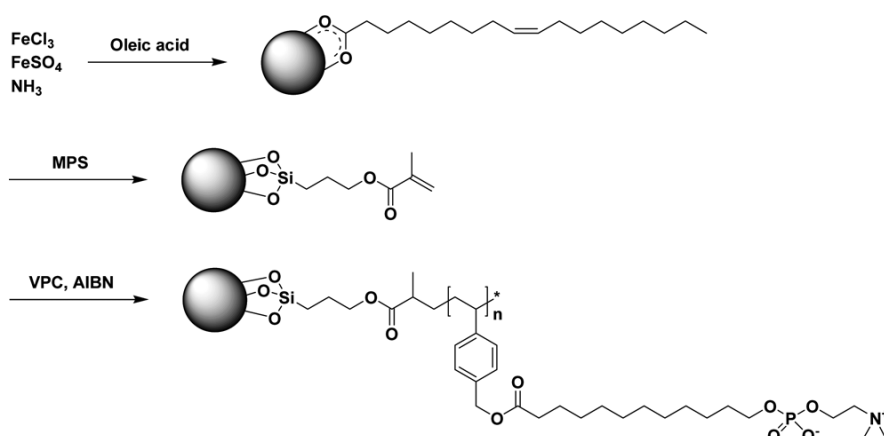


Figure 1.6 Preparation of PC-functionalized MNPs for CRP isolation.²⁵

In 2019, Iwasaki *et al.*²⁶ prepared Poly(MPC)-stabilized Fe_3O_4 nanoparticles (PMPC-MNPs) via hydrothermal method and surface-initiated atom transfer radical polymerization (SI-ATRP) of MPC as shown in **Figure 1.7a**. Aggregation of PMPC-MNPs was induced after incubation with CRP in the presence of Ca^{2+} (**Figure 1.7c**). The size of aggregates as evaluated by dynamic light scattering (DLS) technique was varied as a function of CRP concentration (**Figure 1.7b**). The size change of PMPC-MNPs before and after CRP-induced aggregation as a function of CRP concentration was greater upon the use a neodymium magnet (red circles vs blue circles). The same trend was also observed for the detection in 0.35 g/dL albumin (black triangles). This assay can detect CRP in a range of 0 - 100 nM and a limit of detection of 10 nM.

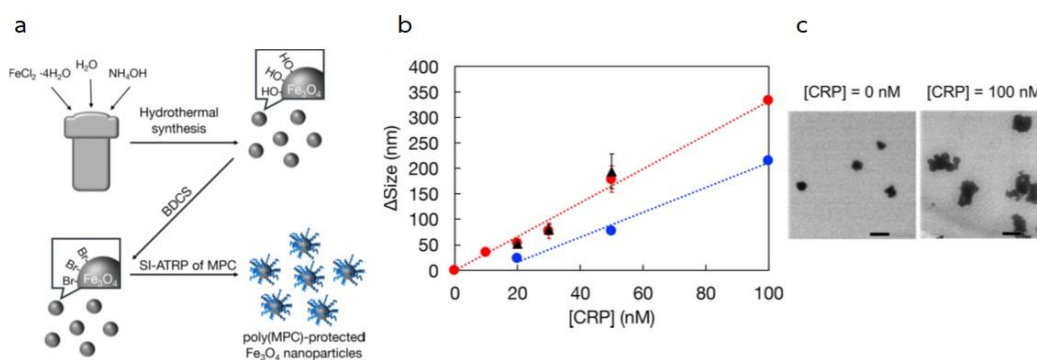


Figure 1.7 (a) Preparation of poly(MPC)-stabilized Fe_3O_4 nanoparticles by hydrothermal treatment and SI-ATRP of MPC. (b) Change in the size of poly(MPC)-stabilized Fe_3O_4 nanoparticles in contact with CRP aggregation of poly(MPC)-stabilized Fe_3O_4 nanoparticles with CRP without (blue circles) and with using a neodymium magnet in buffer (red circles) in 0.35 g/dL albumin (black triangles) and (c) TEM images of poly(MPC)-protected Fe_3O_4 nanoparticles before and after contacting with 100 nM CRP for 60 min.²⁶

Poly[(methacrylic acid)-*ran*-(methacryloyloxyethyl phosphorylcholine)] (PMAMPC) has been introduced recently as an effective stabilizer for MNPs.^{27, 28} The methacrylic acid (MA) repeat units having carboxyl groups allow the copolymer to be easily functionalized²⁹⁻³¹ while the MPC repeat units provide biocompatibility and antifouling characteristics.³²⁻³⁴ The ability of PMPC in preventing nonspecific adsorption in specific detection of antigen–antibody interactions has been continuously demonstrated.³⁵⁻³⁷ Moreover, the specific binding of the PMPC with CRP in the presence of calcium ions was evaluated.

There are many researches that use MNPs nanocomposites to provide peroxidase-like activity in catalytic oxidation of 3,3',5,5'-tetramethylbenzidine (TMB) in the presence of H_2O_2 to develop color reaction^{38, 39} as shown in **Figure 1.8**. MNPs possess an enzyme-mimic activity similar to that of horseradish peroxidase (HRP) and

natural peroxidase.⁴⁰ MNPs offer several advantages over traditional natural enzymes, (a) MNPs exhibit more stable catalytic property than the peroxidases such as HRP, (b) the inherit magnetic separation property of MNPs accommodate magnetic separation and enrichment that are beneficial for biological applications. (c) MNPs can simply be produced at lower cost and less time consuming as opposed to the preparation and purification of natural enzymes. (d) The catalyzed color reaction by MNPs can be performed in a much broader pH range than the standard enzymes and (e) capturing and separating of pathogen from the sample by MNPs can be done with a permanent magnet so that sample preparation can be integrated with a variety of analysis process.^{41, 42}

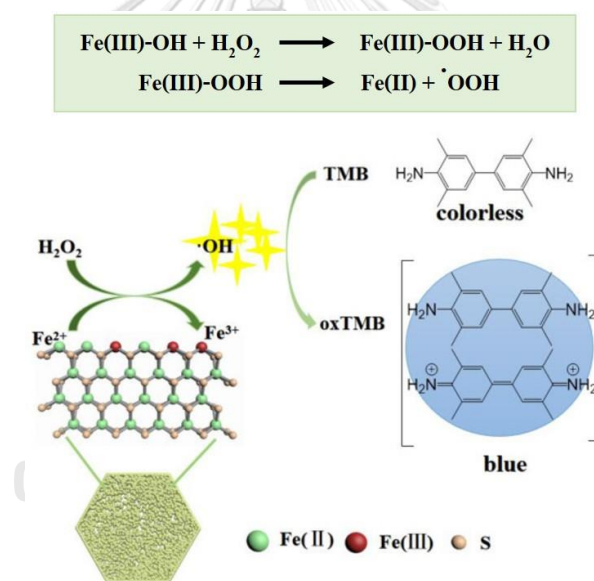


Figure 1.8 Catalytic oxidation by MNPs of TMB which acts as a hydrogen donor for the reduction of H_2O_2 reduction. The resulting diimine leads to the blue solution.⁴³

Many research works have been reported on the use of MNPs nanocomposites to catalyze oxidation of TMB in the presence of H_2O_2 :

In 2013, Woo, *et al.*⁴⁴ detects retroviruses and breast cancer cells by using MNPs nanocomposites. Magnetic nanoparticle (MNP) was immobilized with

monoclonal antibody (MAB), which is specific to retroviruses or breast cancer cells. After the MAb-functionalized MNPs were bound with the target microorganism, TMB and H_2O_2 were added to the sample to produce detection signals, which reflected the amount of retroviruses and breast cancer cells in the sample. The catalytic activity of HRP and MNPs-MAB were compared. It was found that the catalytic activity of MNPs is more stable than HRP.

In 2014, Lui, *et al.*⁴⁵ prepared 5,10,15,20-tetrakis(4-carboxyphenyl-porphyrin)-functionalized Fe_3O_4 nanocomposites ($\text{H}_2\text{T CPP-Fe}_3\text{O}_4$). These nanocomposites exhibited superior peroxidase-like activity to the bare Fe_3O_4 nanoparticles due to their greater affinity toward (Figure 1.9). Colorimetric detection of H_2O_2 showed a dynamic range of 5×10^{-6} - 8×10^{-5} M and detection limit of 1.07×10^{-6} M. Moreover, the same method can be applied for glucose detection of which H_2O_2 was generated by glucose oxidase (GOx) with a dynamic range of 25×10^{-6} - 5×10^{-6} M and detection limit of 2.21×10^{-6} M.

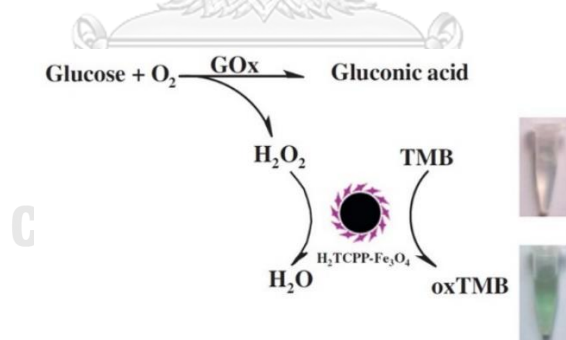


Figure 1.9 Colorimetric glucose detection by using GOx in combination with $\text{H}_2\text{T CPP-Fe}_3\text{O}_4$.⁴⁵

In 2015, Pan, *et al.*⁴⁶ can isolate bacteria strain (designated *Burkholderia sp.* YN01) which was used for the preparation of biogenic Fe_3O_4 MNPs (BMNOs). Peroxidase-like activity of BMNOs was evaluated by using electrochemical analysis and electron spin resonance (ESR) assay. BMNOs were tested for their activity in

degradation of Congo red dye and phenol as well as glucose detection. The catalytic constants (K_{cat}) of H_2O_2 and TMB substrate were $6.5 \times 10^4 \text{ s}^{-1}$ and $0.78 \times 10^4 \text{ s}^{-1}$, respectively which was higher than that of horseradish. The assay can detect H_2O_2 in a range of 0.01 - 8 mM with a detection limit of 0.005 mM. Finally, the glucose was detected in a range of 0.01 - 5 mM and a detection limit of 0.005 mM.

In 2015, Park *et al.*⁴⁷ developed a colorimetric assay for *Salmonella typhimurium* (*S. typhimurium*) detection by using DNA aptamers-modified MNPs (Figure 1.10). Upon an addition of *S. typhimurium* to the solution of DNA aptamers-modified MNPs, specific aptamers on the MNPs would interact with the *S. typhimurium*. Bacteria-bound MNPs nanocomposites were concentrated by a magnet, followed by signal enhancement by the peroxidase activity of the MNPs in the presence of TMB and H_2O_2 .

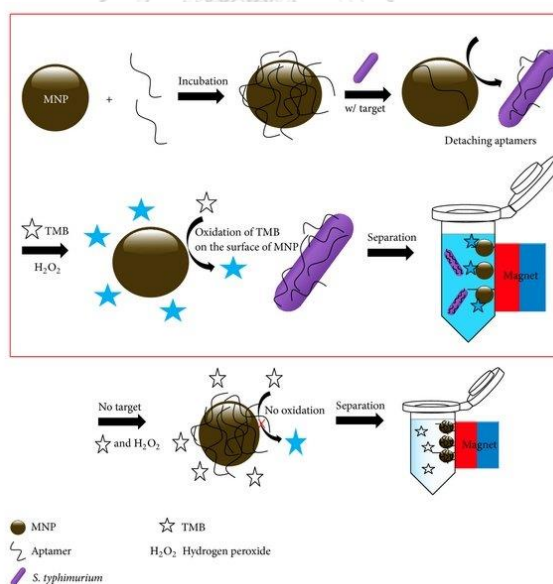


Figure 1.10 MNP-based colorimetric detection of *S. typhimurium* using label-free DNA aptamers and TMB.⁴⁷

In 2016, Zhang et al.⁴⁸ detected *Listeria monocytogenes* (*L. Monocytogenes*) by using aptamer-modified on Fe₃O₄ nanoparticle cluster (NPC) (**Figure 1.11A**) that can be specifically bound to the cell wall of the bacteria. The vancomycin (Van) is a glycopeptide antibiotic for Gram-positive bacteria for capturing *L. Monocytogenes* at different sites. Taking advantage of Fe₃O₄NPC exhibiting ultra-high peroxidase-like activity to create the colored reaction of using TMB/ H₂O₂ as chromogenic substrate as compared with pure Fe₃O₄ nanoparticles (NP) as shown in Figure 1.11B and C, signal amplification of *L. Monocytogenes* can be achieved. The concentration of *L. monocytogenes* corresponds with the absorbance of the colored solution. The assay provided a linear range of of 5.4×10^3 – 10^8 cfu/mL and a limit of detection of 5.4×10^3 cfu/mL.

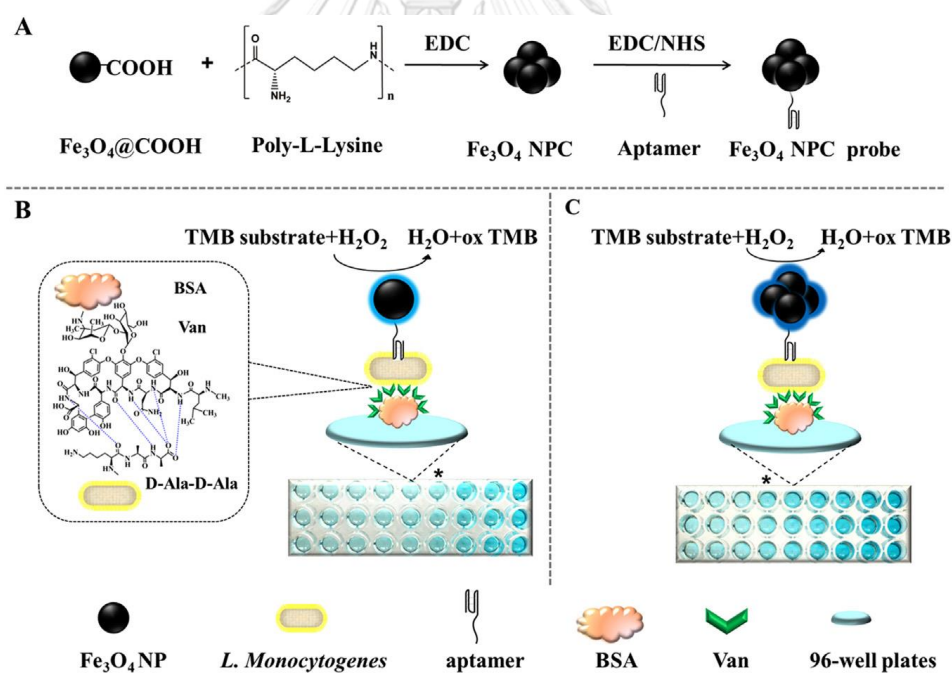


Figure 1.11 (A) Preparation of Fe₃O₄NPC, (B) detection of *L. Monocytogenes* using aptamer-modified Fe₃O₄NPC, and (C) Signal amplification using TMB/H₂O₂ as chromogenic substrate catalyzed by the Fe₃O₄NPC.⁴⁸

Inspired by aforementioned research, the goal of this research is to develop a simple, rapid and effective method for CRP measurement based on magnetic separation of magnetic nanoparticles stabilized with phosphorylcholine-containing polymer, poly[methacrylic acid)-*ran*-(methacryloyloxyethyl phosphorylcholine)] (PMAMPC-MNPs) which were prepared by co-precipitation of ferric and ferrous salts in the presence of PMAMPC. Carboxyl groups in the methacrylic acid (MA) repeat units chelate with Fe atoms during MNPs formation while the methacryloyloxyethyl phosphorylcholine (MPC) repeat units provide biocompatibility, antifouling characteristic, and most importantly, binding sites for CRP in presence calcium ion (Ca^{2+}). The CRP along with PMAMPC-MNPs from tested solution was separated and concentrated upon external magnetic field application. The CRP-unbound PMAMPC-MNPs isolated by external magnet are detected by a label-free colorimetric assay. Taking advantage of peroxidase-like activity of MNPs, the signal was further amplified by introducing TMB as a substrate together with H_2O_2 in CRP-unbound PMAMPC-MNPs solution and was measured by UV-Vis spectroscopy.

1.2 Objectives

1. To prepare and characterize the PMAMPC-MNPs.
2. To study the usage of the PMAMPC-MNPs for detection of CRP.

1.3 Scope of investigation

The stepwise investigation was carried out as follows:

1. Literature survey for related research work.
2. Synthesis and characterization of PMAMPC.
3. Preparation and characterization of PMAMPC-MNPs.
4. Conjugation of PMAMPC-MNPs with CRP.
5. Colorimetric detection of CRP using PMAMPC-MNPs with TMB/ H_2O_2 .

CHAPTER II

EXPERIMENTAL

2.1 Materials

The MPC was purchased from NOF Corp. (Japan), MA supplied by TCI (Japan) was distilled under reduced pressure with added *p*-methoxyphenol (59 °C/13.5 mmHg). Ferrous chloride tetrahydrate ($\text{FeCl}_2 \cdot 4\text{H}_2\text{O}$), ferric chloride hexahydrate ($\text{FeCl}_3 \cdot 6\text{H}_2\text{O}$), calcium chloride (CaCl_2), 3,3',5,5'-tetramethylbenzidine (TMB), hydrogen peroxide (H_2O_2), sodium acetate, C-reactive protein (CRP), human plasma, 4,4'-azobis(4-cyanovaleric acid) (ACVA), 4-cyanopentanoic acid dithiobenzoate (CPD), phosphate buffered saline pH 7.4 (PBS) and dialysis bag (cutoff molecular weight of 3500 g/mol) were purchased from Sigma-Aldrich (USA). Ammonium hydroxide solution (NH_4OH , 28% w/v), ethanol (EtOH) and acetic acid were purchased from Merck (Germany). All reagents and materials are analytical grade and used without further purification. Ultrapure distilled water was obtained after purification using a Millipore Milli-Q system (USA) that involves reverse osmosis, ion exchange and a filtration step.

2.2 Equipments

2.2.1. Attenuated Total Reflectance-Fourier Transform Infrared Spectroscopy (ATR-FTIR)

IR beams are reflected within the ATR crystal and the ATR-FTIR spectra were recorded with a FT-IR spectrometer (Thermo Scientific, Nicolet 6700, USA), model Impact 410, with 32 scans at resolution 4 cm. A frequency of 400-4000 cm was collected by using TGS detector.

2.2.2. Thermogravimetric Analysis (TGA)

Thermogravimetric analysis (TGA) was carried out employing a Diamond TG/DTA (NETZSCH TG 209F3, Germany) and tests were operated under a dynamic nitrogen atmosphere flowing in a temperature range of 30-800°C and the heating rate was set at 10°C/min.

2.2.3. Transmission Electron Microscopy (TEM)

The morphology and actual size of particles were evaluated using transmission electron microscope (TEM, Philips TECNAI 20, UK) operated at 200 kV equipped with 3CCD camera. A sample solution (0.2 mg/ml) in Milli-Q water was directly cast onto carbon-coated copper grids and dried in a desiccator prior to analysis. The Semafore software was used measurement the average diameters from 50 random particles for each sample.

2.2.4. X-ray Diffraction (XRD)

The phase structures of MNPs were characterized by powder X-ray diffraction (XRD, Rigaku, SmartLab 30kV) with Cuka radiation (λ radiation = 0.15418 nm). The measurements were recorded by monitoring the diffraction pattern appearing in the 2θ range from 20-70 degree.

2.2.5. Dynamic Light Scattering (DLS)

The particle size and zeta potential of the MNPs were measured by dynamic light scattering (DLS). The MNPs suspensions were diluted in Milli-Q water and placed into a cuvette. The measurements were taken at 25°C three times for each sample using Malvern Nano ZSP Instruments Ltd., UK to determine the average size distribution and z-average diameter. Zeta potential measurements of these MNPs

suspensions were also determined using the same instrument. The suspensions were diluted with Milli-Q water and added into zeta-cell and measurements were taken three times for each sample at 25°C.

2.2.6. UV-Vis Spectroscopy (UV-Vis)

UV-Vis absorbance measurements of the MNPs suspensions after oxidation with TMB/H₂O₂ solution after 20 min incubation in 96 microplates were done by UV-Vis Spectrophotometer (SpectraMax M2e microplate Reader by Molecular Devices). The experiment was showed in absorbance spectra of a compound in solution.

2.2.7. Nuclear Magnetic Resonance Spectroscopy (NMR)

Crude and pure PMAMPC were characterized by Nuclear Magnetic Resonance Spectroscopy (NMR) in D₂O using a JEOL JNM-ECZ500R/S1 (500 MHz). Percentage of conversion, composition of MA and MPC and degree of polymerization can be calculated from relative peak integration by Mnova version 8.0.

2.3 Experimental Procedure

2.3.1. Synthesis of PMAMPC by RAFT polymerization

PMAMPC having a targeted degree of polymerization (DP) of 100 and the comonomer composition (MA: MPC) of 30:70 was synthesized by RAFT polymerization²⁹ as shown in **Figure 2.1**. The MPC monomer (1.5486 g, 5.24 mmol) was dissolved in 1.87 mL of mixed solvent (1:1, EtOH: 0.1 M PBS in Milli-Q water). After the MPC monomer was completely dissolved, MA monomer (190 µL, 2.20 mmol), ACVA (5.2 mg, 18.70 µmol), and CPD (21 mg, 78.82 µmol), were added to the solution. The RAFT polymerization was operated in a closed system under a nitrogen (N₂) atmosphere by capping the reaction bottle with a septum and the solution was

bubbled with N_2 gas for 30 min and then put in an oil bath at $70\text{ }^\circ\text{C}$ for 6 h. The polymer solution was purified by dialysis in deionized water (DW) for 3 d, filtered by Whatman[®] qualitative filter paper (Grade 1) and then freeze dried before characterized by IR spectroscopy and $^1\text{H-NMR}$ spectroscopy.

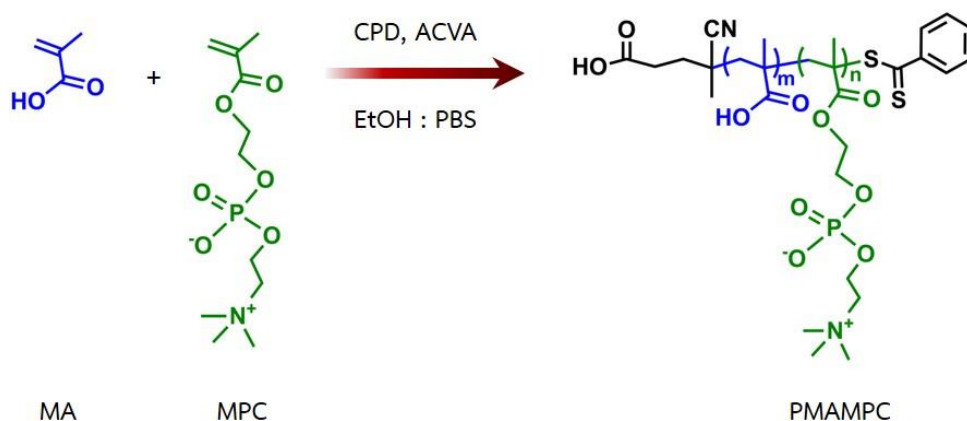


Figure 2.1 Synthesis of PMAMPC by RAFT polymerization.

2.3.2. Preparation of PMAMPC-functionalized MNPs by two-step co-precipitation

PMAMPC was modified on MNPs by two-step co-precipitation²⁷ as shown in **Figure 2.2**. First, FeCl_2 (0.114 g, 0.275 mmol) and FeCl_3 (0.298 g, 0.55 mmol) were dispersed ultrasonically in 10 mL DW for 10 min. Next, the solution was mechanically stirred at speed 750 rpm at 60°C for 30 min under nitrogen atmosphere. Upon an addition of 6 mL ammonia solution (28%w/v), the solution was changed from yellow to black instantly. After 60 min of stirring, the MNPs were formed. After that, a desired amount of PMAMPC (10, 40, 100 and 150 mg) was added in the solution mixture and stirred for 60 min to allow chelation between carboxylic groups of PMAMPC and hydroxy groups on the surface of MNPs. The resulting colloidal PMAMPC-MNPs were separated by external magnetic field and rinsed with DW until

pH of the supernatant became neutral. The colloidal solution of PMAMPC-MNPs was freeze-dried and characterized by ATR-FTIR spectroscopy, TEM, DLS, TGA and XRD.

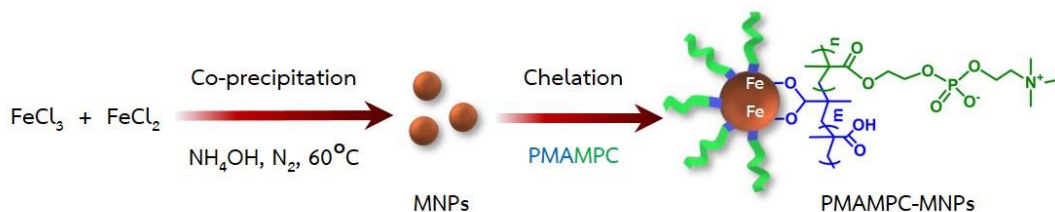


Figure 2.2 Preparation of PMAMPC-functionalized MNPs by two-step co-precipitation.

2.3.3. Colloidal stability of PMAMPC-MNPs

A suspension of PMAMPC-MNPs (0.6 mL, 1.0 mg/mL) prepared using different amount of PMAMPC (10, 40, 100 and 150 mg) was diluted with DW total volume 3 mL. Colloidal stability of the PMAMPC-MNPs suspension was monitored by naked eye observation for 15 min and more than 60 min. The tests were also performed in the presence of calcium choline (CaCl_2) at a time interval of 30 and 60 min. Varied amount of 10 mM CaCl_2 (10, 20 and 30 μL) of were added into PMAMPC-MNPs (40 μL , 1 mg/mL) and the total volume of the solution was adjusted to 100 μL with DW.

2.3.4. Conjugation of PMAMPC-MNPs with CRP

An appropriate amount of PMAMPC-MNPs that can conjugate with CRP and induce the particle precipitation in a timely fashion was first identified. A varied volume (10, 20, 30, 40 μL) of 1 mg/mL PMAMPC-MNPs in aqueous suspension was added with DW to adjust the total volume to 90 μL and followed by an addition of 10 mM CaCl_2 (10 μL). The particle precipitation was observed by naked eyes at 0, 20, 40 and 60 min. A predetermined volume (1.25, 2.5, 5, 10, 15 and 20 μL) of 100 $\mu\text{g}/\text{mL}$ CRP in 0.01 M PBS buffer were added into 1.0 mg/mL PMAMPC-MNPs aqueous suspension of which its optimal quantity was identified above. A 10 μL of 10 mM

CaCl₂ was then introduced and the total volume of the solution was adjusted to 100 μ L. Precipitation of PMAMPC-MNPs in the presence of varied amount of CRP was monitored as a function of time both with and without external magnetic field. To determine specificity of the PMAMPC-MNPs for CRP detection, the same protocol was applied for human serum albumin (HSA) and γ -globulin.

2.3.5. Colorimetric detection of CRP using PMAMPC-MNPs with TMB/H₂O₂

PMAMPC-MNPs (40 μ L, 1mg/mL), a varied volume (1, 2, 3, 4 and 5 μ L) of 100 μ g/mL CRP in 0.01 M PBS buffer (pH 7.4) and CaCl₂ (10 μ L, 10 mM) were added to a 1.5 mL Eppendorf. The total volume was adjusted to 100 μ L with DW and vortex mixed then incubated for 5 min to allow conjugation between PMAMPC-MNPs and CRP. A magnet was then applied under the Eppendorf for 30 sec to induce precipitation. A 50 μ L of supernatant containing unbound PMAMPC-MNPs was taken from the Eppendorf and added into each well of a 96-well microplate containing 197 μ L of 0.1 M acetate buffer (pH 3.8). H₂O₂ (1.53 μ L, 9.8 M) was then added followed by TMB (0.5 μ L, 100 mM) solution in DMSO to obtain a final volume of 250 μ L with DW. The 96-well microplate was shaken on the shaker and incubated at room temperature for 20 min. The absorbance of the solution in the 96-well microplate was measured at 650 nm using UV-vis spectrophotometer (SpectraMax M2/M2e microplate reader). The amount of unbound PMAMPC-MNPs can be calculated from a calibration curve generated from PMAMPC-MNPs of known concentration in a range of 0-5 μ g/mL CRP. The amount of unbound PMAMPC-MNPs is inversely proportional to the amount of CRP.

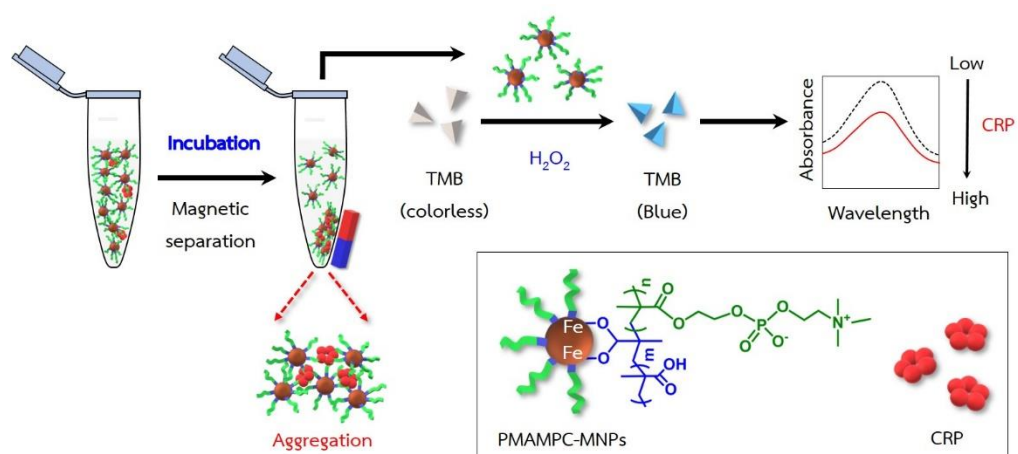


Figure 2.3 Detection of CRP using PMAMPC-MNPs with TMB/H₂O₂.



CHAPTER III

RESULTS AND DISCUSSION

3.1 Preparation and Characterization of PMAMPC-MNPs

PMAMPC was synthesized using RAFT polymerization in the presence of CPD and ACVA as the chain transfer agent (CTA) and radical initiator, respectively that have a targeted degree of polymerization (DP) of 100 and the comonomer composition (MA: MPC) of 30:70. It is anticipated that such DP provides the PMAMPC with high enough molecular size that can provide steric stabilization to the MNPs. The comonomer composition (MA: MPC) of 30:70 should offer enough MA and MPC composition to chelate with Fe atom during MNPs synthesis and binding side with CRP, respectively. The ratio of CTA/initiator or [CTA]/[I] was fixed at 4/1, as previously reported^{27, 29}. From the ¹H-NMR spectrum of PMAMPC (**Figure 3.1**), the characteristic peaks of the MPC unit (-CH₂ (a') = 1.8 ppm, -CH₃ (b') = 0.6-1.4 ppm, -N(CH₃)₃ (c) = 3.15 ppm, -CH₂N (d) = 3.5 ppm, and -POCH₂CH₂N (e) -COOCH₂ (e) -CH₂CH₂OP (e) = 3.8-4.3 ppm) and peaks of MA unit (-CH₂ (a) = 1.8 ppm, -CH₃ (b) = 0.6-1.4 ppm) were clearly observed. Moreover, both spectra of the crude and purified PMAMPC showed signals of dithiobenzoate group at the chain end of PMAMPC (-C₆H₁₁ (f) = 7.4- 7.9 ppm). Only the crude PMAMPC before purification showed vinyl protons of MPC and MA monomers (5.5-6.2 ppm) (**Figure 3.1i**). The fact that such peaks disappeared in the spectrum of purified PMAMPC suggested that unreacted monomers (both MPC and MA) were completely removed after purification. Peak integrations of the proton (H) at 0.6-2.0 ppm and 5.5-6.2 ppm in the spectrum of crude PMAMPC (i) can be used to calculate % conversion using the following equation.

$$\%Conversion = \frac{(peak\ integration\ at\ 0.6 - 2.0)/5}{(peak\ integration\ at\ 0.6 - 2.0)/5 + (peak\ integration\ at\ 5.5 - 6.2)/5} \times 100 \quad (3.1)$$

According to the calculation, % conversion was found to be 94%. The degree of polymerization (DP) which is equivalent to total repeating unit and the composition of MPC and MA in the PMAMPC can be calculated using **equation 3.2-3.6**.

$$Total\ repeating\ unit\ (A) = \frac{(peak\ integration\ at\ 0.6 - 1.4\ ppm)/3}{(peak\ integration\ at\ 7.4 - 7.9\ ppm)/5} \quad (3.2)$$

$$MPC\ unit\ (B) = \frac{(peak\ integration\ at\ 3.15\ ppm)/9}{(peak\ integration\ at\ 7.4 - 7.9\ ppm)/5} \quad (3.3)$$

$$MA\ unit\ (C) = A - B \quad (3.4)$$

$$MPC\ composition\ (\%) = \frac{100B}{A} \quad (3.5)$$

$$MA\ composition\ (\%) = \frac{100C}{A} \quad (3.6)$$

The copolymer composition (MA: MPC) determined from the 1H -NMR spectrum was 25:75 with a DP of 102. The calculated molecular weight of PMAMPC was found to be 25 kDa. The copolymer composition and molecular weight determined by 1H -NMR closely resembled the expected theoretical values, suggesting that the copolymerization was relatively well-controlled.

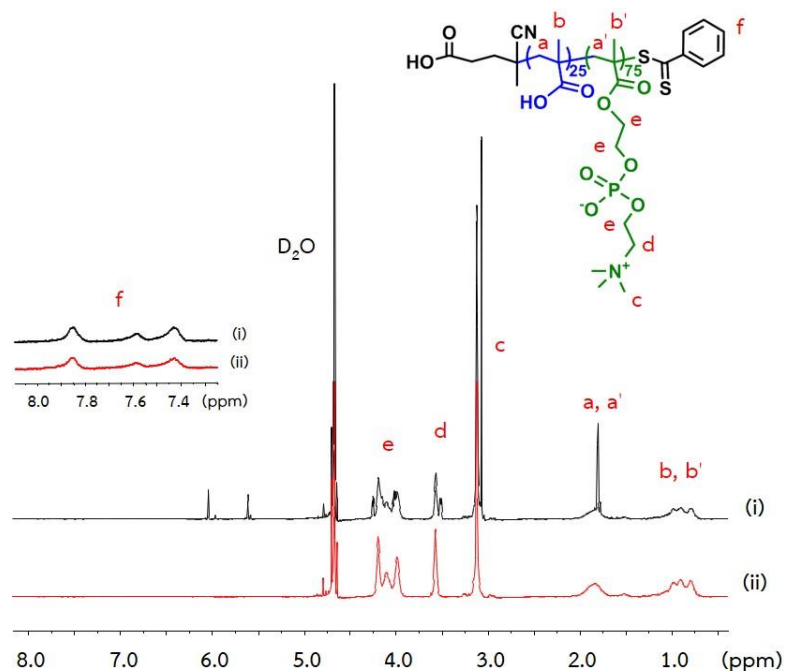


Figure 3.1 ¹H-NMR spectra of (i) crude and (ii) purified PMAMPC.

PMAMPC-MNPs were prepared by the two-step co-precipitation following the published procedure^{27, 29}. The surface modification of MNPs with PMAMPC was verified by ATR-FTIR. As shown in **Figure 3.2**, a characteristic Fe-O vibration of the unmodified MNPs was observed at 550 cm⁻¹ in both unmodified MNPs (a) and PMAMPC-MNPs (b-f). Bands at 953, 1053 and 1715 cm⁻¹, assignable to N⁺(CH₃)₃, P-O and C=O stretching, respectively apparently emerged in the spectra of PMAMPC-MNPs prepared by using 100 and 150 mg of PMAMPC (d and e) which coincided with PMAMPC (f). Such peaks were absent in the spectra of PMAMPC-MNPs prepared by using 10 and 40 mg of PMAMPC (b and c). This may be explained as a result of the PMAMPC of 40 mg and below is too low to be detectable by ATR-FTIR.

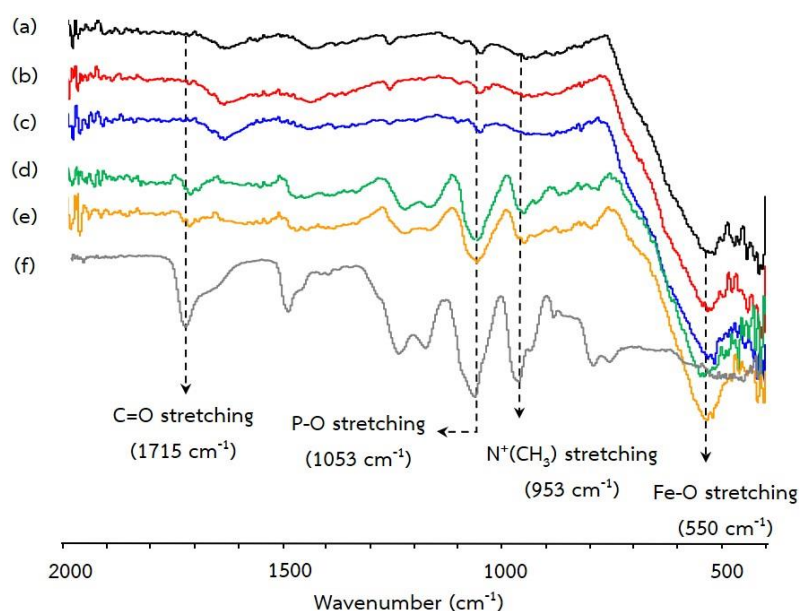


Figure 3.2 ATR-IR spectra of (a) bare MNPs, PMAPMC-MNPs prepared by using PMAMPC of (b) 10, (c) 40, (d) 100, and (e) 150 mg and (f) PMAMPC.

The colloidal stability of the PMAMPC-MNPs as a function of time as shown in **Figure 3.3** agrees quite well with the ATR-FTIR analysis in that 10 and 40 mg of PMAMPC were certainly not enough to yield stable PMAMPC-MNPs. Similar to the uncoated MNPs, the PMAMPC-MNPs prepared from those PMAMPC quantity precipitated after 15 min. In contrast, the PMAMPC-MNPs prepared from 100 mg PMAMPC remained stable more than 60 min (for up to 1 month) implying that such quantity was enough to provide steric stabilization to the MNPs and preventing them from precipitation. Elevating the amount of PMAMPC to 150 mg, however, yielded PMAMPC-MNPs with inferior dispersibility. Precipitation took place at 60 min. For this reason, PMAMPC-MNPs prepared using 100 mg PMAMPC was chosen for further investigation.

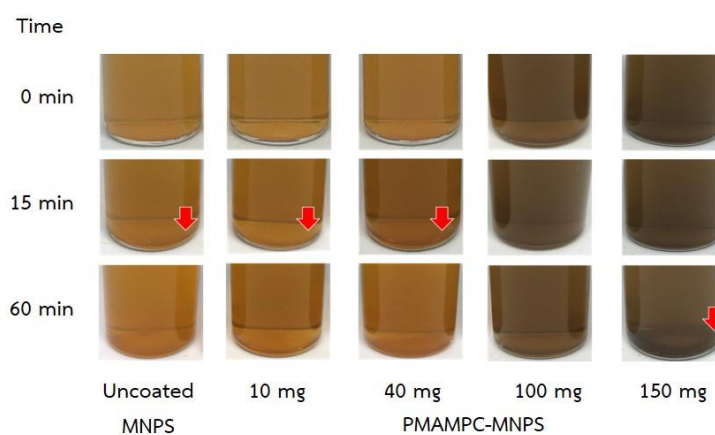


Figure 3.3 Appearance of aqueous dispersion of bare MNPs and PMAMPC-MNPs prepared using varied PMAMPC quantity as a function of time.

The crystallographic structure and composition of the PMAMPC-MNPs were identified by XRD of which patterns are shown in **Figure 3.4**. The diffraction peaks of bare MNPs appeared at 30.04° (2 2 0), 35.33° (3 1 1), 43.06° (4 0 0), 53.51° (4 2 2), 57.09° (5 1 1) and 62.71° (4 4 0), which were consistent with the literature values of standard Fe_3O_4 crystals with inverse spinel structure.^{49, 50} Apparently, the PMAMPC coating did not have noticeable impact on the MNPs crystallographic structure⁵¹.

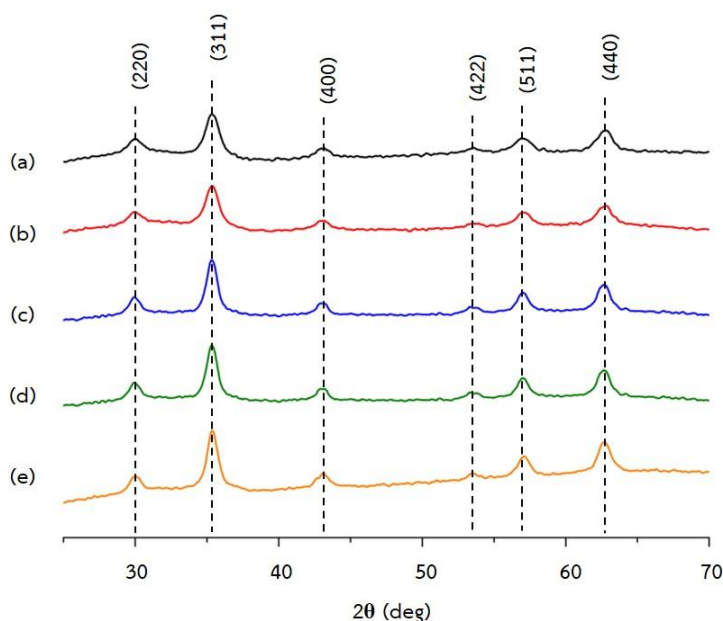


Figure 3.4 XRD spectra of (a) bare MNPs, PMAPMC-MNPs prepared by using PMAMPC of (b) 10, (c) 40, (d) 100, and (e) 150 mg.

Figure 3.5 shows the TGA curves of the PMAPMC-MNPs in comparison with bare MNPs. The first weight loss of all MNPs took place about 100°C as a result of dehydration. PMAPMC-MNPs prepared by using PMAMPC of 40 mg showed the highest weight loss of about 3.21%, implying that they contained the greatest of bound water content. The second weight loss occurring in a temperatures range of 300 - 400°C could be ascribed to the decomposition of PMAMPC bonded to MNPs.^{27, 52, 53} The greater weight loss of 6.62 and 7.16% of PMAPMC-MNPs prepared by using 100 and 150 mg, respectively than that of bare MNPs (5.59%), PMAPMC-MNPs prepared by using 10 (5.50%) and 40 (6.17%) mg confirmed the presence of varied amount PMAMPC on MNPs. The third weight loss appearing at the highest temperature (>730°C) for the PMAPMC-MNPs prepared by using 100 and 150 mg. This should be a contribution of char of macromolecular organic content (PMAMPC) on the PMAPMC-MNPs because such weight loss was absent in the curves of bare

MNPs and PMAMPC-MNPs prepared by using low quantity of PMAMPC (10 and 40 mg).

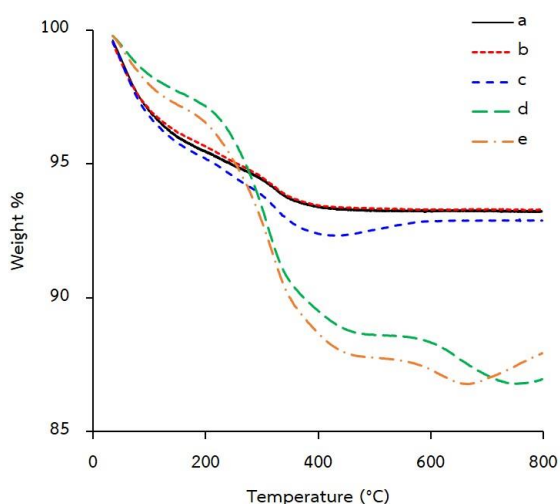


Figure 3.5 TGA (under N_2) curves of (a) bare MNPs, PMAMPC-MNPs prepared by using PMAMPC of (b) 10, (c) 40, (d) 100, and (e) 150 mg with a heating rate of $20^\circ\text{C}/\text{min}$.

3.2 Conjugation of PMAMPC-MNPs with CRP

Various concentration of CaCl_2 in a range of 1 – 3 mM was added into 0.4 mg/ml PMAMPC-MNPs aqueous suspension. As shown in **Figure 3.6**, the PMAMPC-MNPs solution had good colloidal stability in the presence of Ca^{2+} of 1 and 2 mM for up to 60 min. Precipitation of PMAMPC-MNPs (0.4 mg/mL) prepared using 100 mg PMAMPC was observed when the CaCl_2 concentration reached 3 mM at 60 min. To minimize the risk of Ca^{2+} -induced precipitation of the PMAMPC-MNPs even without CRP, CaCl_2 of 1 mM was chosen for CRP detection.

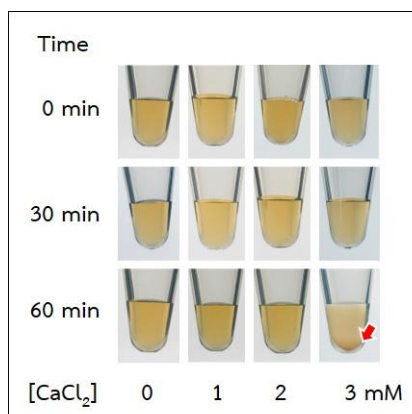


Figure 3.6 Appearance of colloidal PMAMPC-MNPs (0.4 mg/mL) in the presence of varied CaCl_2 concentration as a function of incubation time.

Specific binding of CRP (20 $\mu\text{g/mL}$) was tested with PMAMPC-MNPs of varied concentration (0.1, 0.2, 0.3 and 0.4 mg/mL) in the presence of 1 mM Ca^{2+} . As shown in **Figure 3.7**, no sedimentation of 0.1 mg/mL PMAMPC-MNPs was observed even in the presence of CRP implying that the PMAMPC-MNPs concentration was too low. The addition of CRP that can bind with PMAMPC-MNPs induced precipitation of 0.2 and 0.3 mg/mL PMAMPC-MNPs after 40 min of incubation. The CRP-induced precipitation of 0.4 mg/mL PMAMPC-MNPs happened in a shorter period of incubation (20 min). The concentration of 0.4 mg/mL was therefore chosen as an optimal PMAMPC-MNPs concentration to be used for CRP detection.

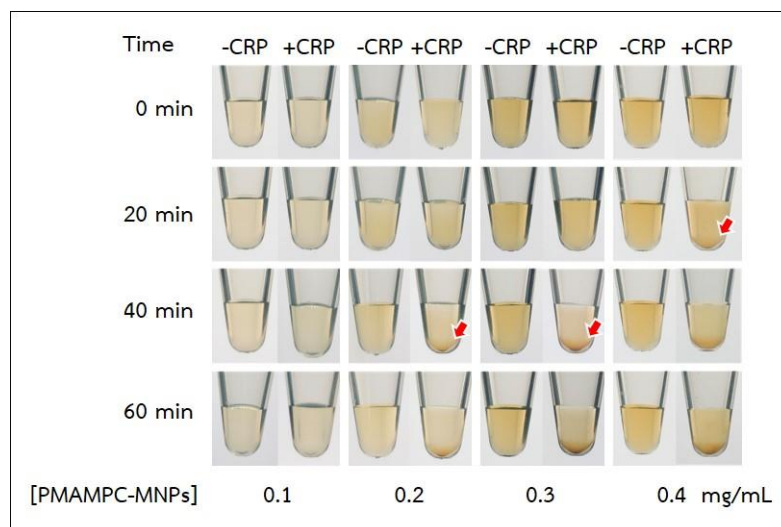


Figure 3.7 Appearance of colloidal PMAMPC-MNPs of varied concentration before and after the addition of CRP (20 $\mu\text{g}/\text{mL}$) in the presence of 1 mM Ca^{2+} as a function of incubation time.

Upon using 1 mM of Ca^{2+} and 0.40 mg/mL PMAMPC-MNPs, the conjugation of PMAMPC-MNPs with CRP of varied concentration that can induce precipitation without external magnetic field application as a function of time was investigated. The results shown in **Figure 3.8a** demonstrate that the precipitation occurred more rapidly in the presence of 10 $\mu\text{g}/\text{mL}$ CRP or higher than those of lower CRP concentration. A minimum concentration of CRP that can induce precipitation within a reasonable period of time (40 min) was 5 $\mu\text{g}/\text{mL}$. The conjugation was also performed with human serum albumin (HSA) and γ -globulin for comparison. As illustrated in **Figure 3.8b**, precipitation was not observed upon the addition of HSA and γ -globulin as opposed to CRP, suggesting the specificity of PMAMPC-MNPs towards CRP and verifying antifouling characteristic of the PMAMPC against other non-specific proteins. Effect of external magnetic field on the CRP conjugation on PMAMPC-MNPs was also investigated. The results shown in **Figure 3.8c** indicated that the precipitation of PMAMPC-MNPs in the presence of Ca^{2+} and CRP was accelerated

under the external magnetic field which happened within 30 sec. Only small amount of PMAMPC-MNPs was found precipitated in the absence of CRP.

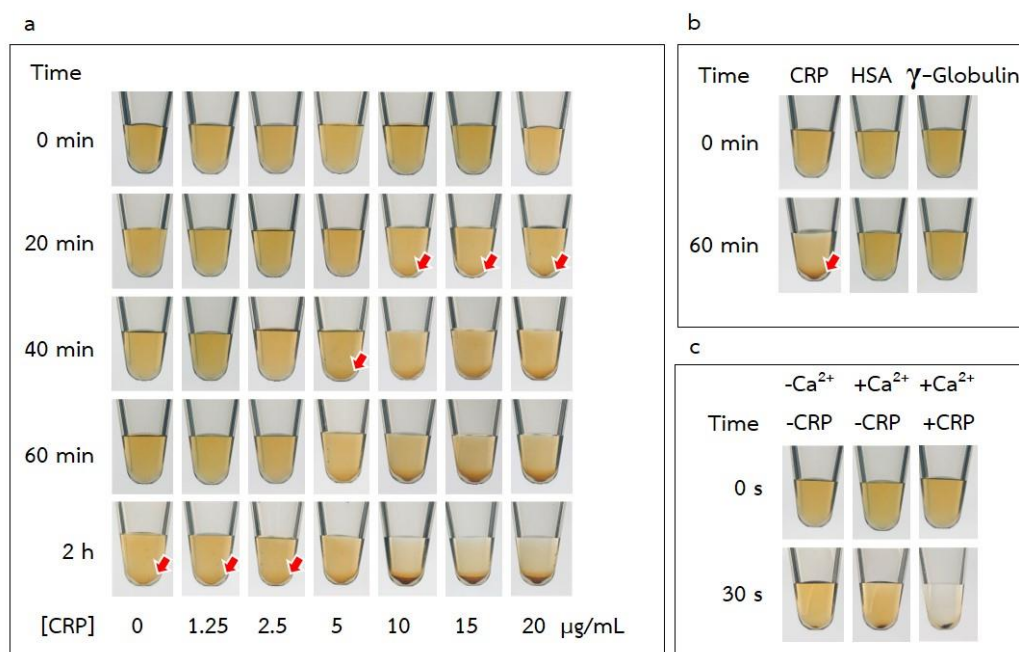


Figure 3.8 Appearance of colloidal PMAMPC-MNPs upon an addition of (a) varied CRP concentration as a function of time, (B) CRP in comparison with HSA and γ -globulin, (C) Ca²⁺ and Ca²⁺ together with CRP under the external magnetic field.

The hydrodynamic diameter and zeta potential (ζ) PMAMPC- MNPs were determined by DLS. As shown in **Figure 3.9a**, the hydrodynamic radius of bare MNPs was 796 ± 182 nm with broad polydispersity index or PDI (0.837). These data strongly indicate that aqueous dispersibility of the bared MNPs was poor so that extensive agglomeration was observed. The diameter of PMAMPC-MNPs decreased to 140.5 ± 3.6 nm (PDI = 0.208). This much smaller hydrodynamic dimension with much narrower dispersity suggested that PMAMPC was an effective stabilizing agent that can provide both steric stabilization and charge repulsion from the negatively charged carboxyl groups of MA units in the copolymer. The latter effect can be verified from the more negative zeta potential value of the PMAMPC-MNPs ($-21.6 \pm$

2.21 mV) as opposed to the bare MNPs (3.99 ± 0.34 mV). Upon conjugation with CRP, the hydrodynamic size of PMAMPC-MNPs became larger to 934.4 ± 82.1 nm (PDI = 0.260) as a consequence of agglomeration. The isoelectric point of CRP is approximately 6.3⁵⁴ which should result in CRP being positively charged in DW (pH 5.5-6.5). As a result, the zeta potential of the PMAMPC-MNPs became less negative (-8.96 ± 1.52 mV).

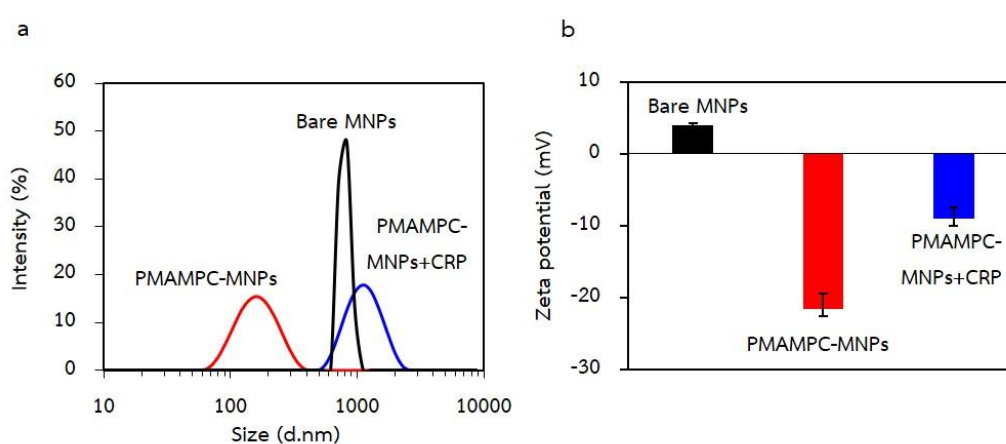


Figure 3.9 (a) DLS profiles and (b) zeta potential values of bare MNPs and PMAMPC-MNPs both before and after the addition of CRP ($5 \mu\text{g/mL}$) in the presence of 1 mM Ca^{2+} .

Figure 3.10 shows the morphology of bare MNPs, PMAPMC-MNPs both before and conjugation with CRP as determined by TEM. The bare MNPs (**Figure 3.10a**) showed a certain degree of agglomeration due to its poor aqueous dispersity. An average diameter of individual particle of 9.56 ± 1.63 nm was calculated. Less aggregation was observed for PMAPMC-MNPs, of which diameter became slightly larger to 12.81 ± 2.71 nm as a result of PMAPMC coating (**Figure 3.10b**). After conjugating with CRP, extensive agglomeration was also realized. This may be ascribable to the conjugation with relatively large molecule of CRP (115 kDa).^{12, 55} The average diameter of individual PMAPMC-MNPs was unaffected by CRP conjugation

(Figure 3.10c). Results from TEM analysis apparently agree very well with the data obtained from DLS analysis.

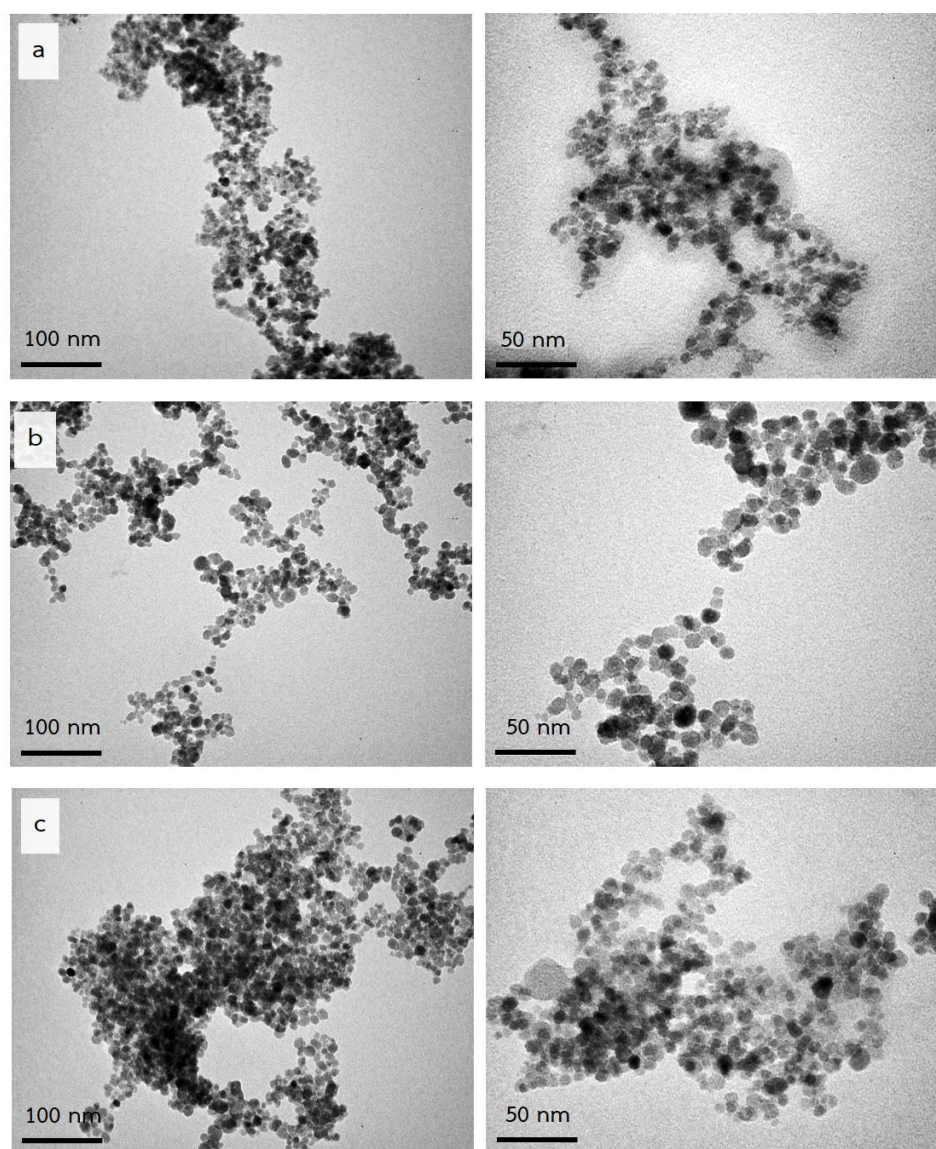


Figure 3.10 TEM micrographs of (a) bare MNPs, PMAPMC-MNPs both (b) before and (c) after conjugation with CRP (5 $\mu\text{g}/\text{mL}$) in the presence of 1 mM Ca^{2+} . (Scale bar = 100 nm (left) and 50 nm (right)).

3.3 Colorimetric detection of CRP using PMAMPC-MNPs with TMB/H₂O₂

The peroxidase catalytic activity behavior was examined by the oxidation reaction of TMB in the presence of H₂O₂ catalyzed by PMAMPC-MNPs. The peroxidase-like activity was measured by monitoring a blue color of oxidized TMB of which the color intensity was directly proportional to catalytic activity which should be varied as a function the PMAMPC-MNPs quantity. As shown in **Figure 3.11**, PMAMPC-MNPs could catalyze the oxidation of TMB substrate producing a blue color solution detectable by UV-Vis spectroscopy at 650 nm only in the presence of both TMB and H₂O₂. With either TMB or H₂O₂ alone, blue color was not developed implying the catalytic oxidation did not take place. There was also no background color from a combination of TMB and H₂O₂ suggesting that the blue color development happened as a result of the peroxidase-like activity of PMAMPC-MNPs in the presence of TMB and H₂O₂. After CRP conjugation, part of PMAMPC-MNPs were precipitated, only unbound PMAMPC-MNPs that remained in the supernatant provided peroxidase-like activity so that the developed blue color was less in intensity as compared with the PMAMPC-MNPs before CRP conjugation.

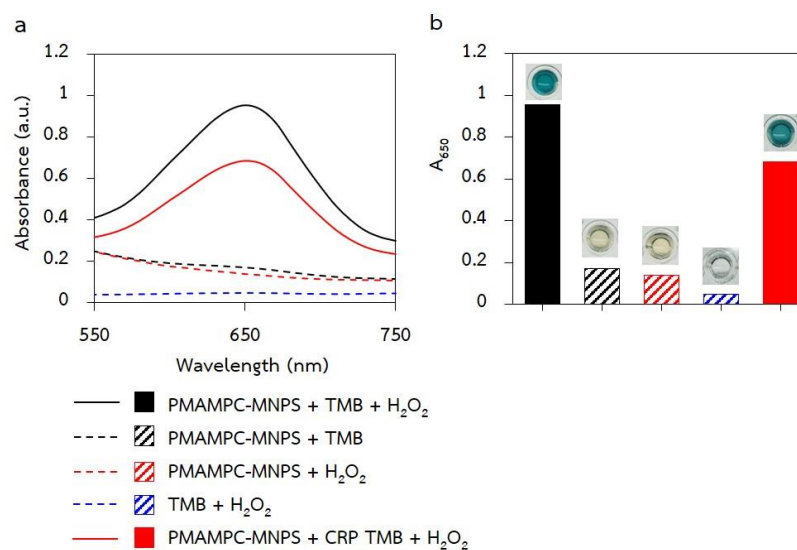


Figure 3.11 UV-Vis absorption (a) spectra and (b) bar graphs of UV-Vis absorbance at 650 nm of PMAMPC-MNPs + TMB + H₂O₂ (black solid line and black filled strip), PMAMPC-MNPs + TMB (black dashed line and black pattern), PMAMPC-MNPs + H₂O₂ (red dashed line and red pattern), TMB + H₂O₂ (blue dashed line and blue pattern), and PMAMPC-MNPs + CRP + TMB + H₂O₂ (red solid line and red filled strip). The insets in (b) show appearance of solution in the well plates.

Conjugation of PMAMPC-MNPs with CRP of varied concentration in a range of 0 – 5 $\mu\text{g/mL}$ was determined. **Figure 3.12a** shows the intensity of the blue color solution produced by unbound PMAMPC-MNPs in the supernatant after the PMAMPC-MNPs conjugated with CRP being separated by the external magnetic field. The intensity of colored solution was found to decrease linearly with CRP concentration that has a linear range of 0 - 5 $\mu\text{g/mL}$ ($y = -0.1658x + 1.7995$, $R^2 = 0.9842$). Limit of detection (LOD) of the method which is the lowest detectable CRP concentration can be estimated from color intensity at least three times higher than the standard deviation of the background (0 $\mu\text{g/mL}$) using **equation 3.7**. At 0 $\mu\text{g/mL}$, intensity was found to be 1.7612 ± 0.0766 . LOD which is three times SD dividing slope (m) can be calculated as 1.39 $\mu\text{g/mL}$.

$$x = \frac{3SD_0}{m} \quad (3.7)$$

I_{LOD} represents the intensity at LOD whereas I_0 reflects the intensity of the background and SD_0 is standard deviation of the background. After that, LOD was calculated from I_{LOD} using linear equation of the calibration curve.

Moreover, the detection of 3 $\mu\text{g/mL}$ CRP in rabbit serum solution was also performed. **Figure 3.12b** showed the intensity of the blue color solution produced by the unbound PMAMPC-MNPs before and after CRP conjugation. The intensity of blue color solution of the unbound PMAMPC-MNPs before CRP conjugation in 50% diluted and undiluted rabbit serum solutions were found to be lower than that in aqueous solution. This may be explained as a result of proteins in the undiluted rabbit serum deteriorated the catalytic activity of the PMAMPC-MNPs to some extent. After CRP conjugation, the intensity of the blue color solution was proportionally decreased as anticipated. It was found that ratio of the intensity of the blue color solution produced by the unbound PMAMPC-MNPs before and after CRP conjugation was approximately 1.3-1.4 in all solutions (aqueous solution, in 50% diluted and undiluted rabbit serum solutions). This similar ratio suggests that this assay is applicable for CRP detection in both serum-free and undiluted plasma.

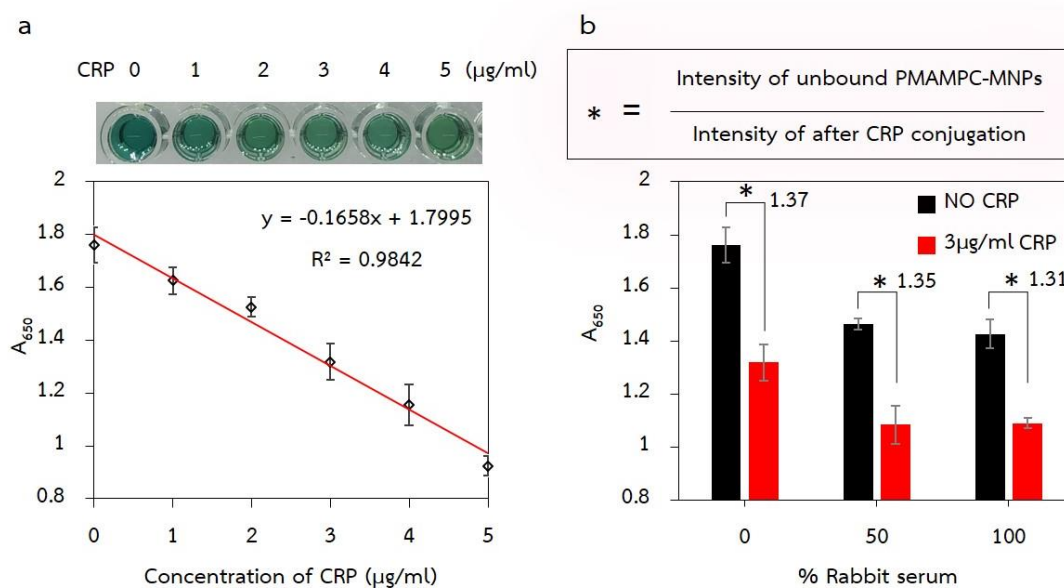


Figure 3.12 (a) A calibration plot of UV-Vis absorbance as a function of CRP concentration and solution of unbound PMAMPC-MNPs after oxidation with TMB and H_2O_2 . (b) UV-Vis absorbance of solution produced by the unbound PMAMPC-MNPs before and after CRP conjugation.

The comparison of the analytical performance between this sensor and other sensors is presented in **Table 3.1**. In general, antibody-based sensors (entry 3-6) offer high specificity as well as sensitivity. LODs are in a range of ng/mL. However, using antibody is quite costly and has limited stability. PC group have been introduced as an alternative non-antibody probe that is quite efficient. By employing PC-BSA-conjugated carboxylated microspheres, the detection via turbidimetric and ELISA assay (entry 1-2) provided a linear range of 0.5 – 10 and 0 – 10 $\mu\text{g/ml}$, respectively which cover a concentration of 3 $\mu\text{g/ml}$, the risk value for cardiovascular disease. PMPC having multiple PC groups along the chain was also applied as probes for CRP detection (entry 7-9). As anticipated, electrochemical detection using differential pulse voltammetry (DPV) offers the lowest LOD (1.55×10^{-3} $\mu\text{g/ml}$) in comparison with localized surface plasmon resonance (LSPR) and dynamic light scattering (DLS).

However, the risk value for cardiovascular disease falls in the linear ranges obtained for all techniques (DPV, LSPR, and DLS).

From this study, it can be seen that the use of colorimetric assay based on PMAMPC-MNPs exhibits equivalent performance in terms of LOD (1.39 $\mu\text{g/mL}$) to ELISA assay based on PC-BSA-conjugated carboxylated microspheres and a similar linear range of detection as those based on PC-BSA-conjugated carboxylated microspheres via turbidimetric and ELISA assay (entry 1-2). In comparison with other assays employing MNPs, the PMAMPC-MNPs are superior to polyclonal goat anti-CRP (covalently) bound MNPs (entry 5) since they are antibody-free and also provide a broader linear range of CRP detection. The colorimetric assay based on PMAMPC-MNPs showed a similar LOD to that of PMPC- Fe_3O_4 -based DLS analysis (1.15 $\mu\text{g/mL}$) (entry 8). Nevertheless, the preparation for PMAMPC-MNPs by the two-step coprecipitation is much simpler and less sophisticated than the method used for PMPC- Fe_3O_4 preparation which is based on co-precipitation followed by surface-initiated polymerization. Besides, the colorimetric method can be easily implemented for an on-site detection as opposed to DLS analysis since no specific instrument is required.

Table 3.1 Analytical characteristics of different CRP biosensors previously reported.

Entry	Assay type	Materials/Substrate	Liner range ($\mu\text{g/mL}$)	LOD ($\mu\text{g/mL}$)	Reference
1	Turbidimetric method	PC-BSA -conjugated carboxylated microspheres	0.5 - 10	-	Deegan et al. (2003) ⁵⁶
2	Enzyme linked absorbance assay (ELISA)	PC-BSA -conjugated carboxylated microspheres	0 - 10	1.06	Deegan et al. (2003) ⁵⁶
3	Immunoassay (Agglutination)	Anti-CRP (monoclonal antibody) immobilized MPC-PNPs	1 - 1,000	-	Park et al. (2004) ¹⁸
4	Nephelometric method	Anti-CRP bound polystyrene bead and acridinium-labeled anti-CRP	0.01 - 50	4.0×10^{-3}	Shiesh et al. (2006) ⁵⁷
5	Immunomagnetic reduction (IMR)	Polyclonal goat anti-CRP (covalently) bound MNPs	0.1 - 1	-	Chang et al. (2012) ⁵⁸
6	Sandwich nanoparticle immunoassay	anti-CRP modified iron oxide @SiO ₂ and (CdSe/ZnS)@SiO ₂	0.00118 - 11.8	1.0×10^{-3}	Yang et al. 2014 ²⁴
7	Localized surface plasmon resonance (LSPR)	PMPC-b-PMAT-SH modified AUNPs	0 - 9.5	2.3 - 4.7	Iwasaki et al. (2014) ¹⁹
8	Dynamic Light Scattering (DLS)	PMPC-Fe ₃ O ₄	0 - 69	1.15	Iwasaki et al. (2019) ⁵⁶
9	Differential pulse voltammetry (DPV)	PMPC-SH modified AUNPs-SPCE/PADS	0.005 - 5	1.55×10^{-3}	Pinyorospatham et al. (2019) ²⁰
10	Colorimetric method	PMAMPC-MNPs	0 - 5	1.39	This work

CHAPTER IV

CONCLUSION AND SUGGESTIONS

The present study has demonstrated that PMAMPC can be synthesized by RAFT polymerization. The copolymer composition (MA: MPC) determined from the $^1\text{H-NMR}$ spectra was 25:75 with the DP of 102. The calculated molecular weight of PMAMPC was found to be 25 kDa. The PMAMPC-MNPs can be prepared by the two-step co-precipitation. Characteristic peaks of PMAMPC on the PMAMPC-MNPs were verified by ATR-IR spectroscopy. According to XRD analysis, the coating of PMAMPC did not affect the crystal structure of MNPs which appeared to match the standard Fe_3O_4 crystals as anticipated. TGA data suggested that the amount of organic content on the PMAMPC-MNPs is proportional to the PMAMPC used in the step of co-precipitation. Colloidal stability test suggested that PMAMPC-MNPs prepared using 100 mg PMAMPC were the most suitable particles used for further studies as they remained stable for up to 1 month.

The 1 mM of Ca^{2+} and 0.40 mg/mL PMAMPC-MNPs were found to be the appropriate amount for testing specific conjugation with CRP. Without the external magnetic application, a minimum concentration of CRP that can induce precipitation of PMAMPC-MNPs within a reasonable period of time (40 min) was 5 $\mu\text{g/mL}$. The precipitation was accelerated under the external magnetic field which happened within 30 sec. The precipitation was not observed upon the addition of HSA and γ -globulin as opposed to CRP, suggesting the specificity of PMAMPC-MNPs towards CRP and verifying antifouling characteristic of the PMAMPC against other non-specific proteins. PMAMPC-MNPs both before and after specific conjugation with CRP in the presence of Ca^{2+} was microscopically confirmed by both DLS and TEM analysis. As evaluated by TEM, an average diameter of 12.81 ± 2.71 nm was found for PMAPMC-

MNPs which were slightly larger than that of bared MNPs (9.56 ± 1.63 nm) implying the presence of PMAMPC coating. The diameter of individual PMAMPC-MNPs was unaffected by CRP conjugation. Apparently, PMAMPC-MNPs were much more dispersed with lower hydrodynamic radius (140.5 ± 3.6 nm, PDI = 0.208) than the bared MNPs (796 ± 182 nm, PDI = 0.837) as verified by DLS. Upon conjugation with CRP, the hydrodynamic size of PMAMPC-MNPs became larger to 934.4 ± 82.1 nm (PDI = 0.260). The more negative zeta potential value of the PMAMPC-MNPs (-21.6 ± 2.21 mV) became less negative (-8.96 ± 1.52 mV) once conjugated with positively charged CRP.

The PMAMPC-MNPs can be used for the detection of CRP using magnetic separation. The external magnetic field was applied to induce precipitation of PMAMPC-MNPs along with CRP from the tested solution. The unbound PMAMPC-MNPs in the supernatant was then detected by the label-free colorimetric assay. Taking advantage of peroxidase-like activity of PMAMPC-MNPs, the signal was further amplified by introducing TMB as a substrate together with H_2O_2 and was measured by UV-Vis spectroscopy. Optimized condition for the colorimetric detection via TMB oxidation was using acetate buffer at pH 3.8, TMB concentration of $200 \mu\text{M}$, H_2O_2 concentration of 80 mM and incubation time of 20 min. The intensity of the blue-colored solution decreased linearly as a function of CRP in a concentration range of $0\text{-}5 \mu\text{g/mL}$ and detection limit of $1.39 \mu\text{g/mL}$. Finally, we can detect $3 \mu\text{g/mL}$ (risk value of cardiovascular disease) in undiluted rabbit serum.

REFERENCES

1. Upadhyay, R. K., Emerging Risk Biomarkers in Cardiovascular Diseases and Disorders. *J Lipids* **2015**, *2015*, 971453-971503.
2. Sproston, N. R.; Ashworth, J. J., Role of C-Reactive Protein at Sites of Inflammation and Infection. *Front Immunol* **2018**, *9*, 754.
3. Eisenhardt, S. U.; Thiele, J. R.; Bannasch, H.; Stark, G. B.; Peter, K., C-Reactive Protein: How Conformational Changes Influence Inflammatory Properties. *Cell Cycle* **2009**, *8* (23), 3885-92.
4. Thiele, J. R.; Zeller, J.; Bannasch, H.; Stark, G. B.; Peter, K.; Eisenhardt, S. U., Targeting C-Reactive Protein in Inflammatory Disease by Preventing Conformational Changes. *Mediators Inflamm* **2015**, *2015*, 372432.
5. Osman, R., L'Allier, P. L., Elgharib, N., & Tardif, J. C., Critical Appraisal of C-Reactive Protein Throughout the Spectrum of Cardiovascular Disease. *Vasc Health Risk Manag* **2006**, *2* (3), 221-237.
6. Pearson, T. A.; Mensah, G. A.; Alexander, R. W.; Anderson, J. L.; Cannon, R. O., 3rd; Criqui, M.; Fadl, Y. Y.; Fortmann, S. P.; Hong, Y.; Myers, G. L.; Rifai, N.; Smith, S. C., Jr.; Taubert, K.; Tracy, R. P.; Vinicor, F.; Centers for Disease, C.; Prevention; American Heart, A., Markers of Inflammation and Cardiovascular Disease: Application to Clinical and Public Health Practice: A Statement for Healthcare Professionals from the Centers for Disease Control and Prevention and the American Heart Association. *Circulation* **2003**, *107* (3), 499-511.
7. Mali, B.; Armbruster, D.; Serediak, E.; Ottenbreit, T., Comparison of Immunoturbidimetric and Immunonephelometric Assays for Specific Proteins. *Clin Biochem* **2009**, *42* (15), 1568-71.
8. Drieghe, S. A.; Alsaadi, H.; Tugirimana, P. L.; Delanghe, J. R., A New High-Sensitive Nephelometric Method for Assaying Serum C-Reactive Protein Based on Phosphocholine Interaction. *Clin Chem Lab Med* **2014**, *52* (6), 861-7.
9. Tugirimana, P. L.; De Clercq, D.; Holderbeke, A. L.; Kint, J. A.; De Cooman, L.; Deprez, P.; Delanghe, J. R., A Functional Turbidimetric Method to Determine C-Reactive

Protein in Horses. *J Vet Diagn Invest* **2011**, *23* (2), 308-311.

10. Correia, C. L.; Lima, J. C.; Gerstenblith, G.; Magalhães, L. P.; Moreira, A.; Jr., B.; Octávio, D. J.; Passos, L. C. S.; D'Oliveira, J. A.; Esteves, J. P., Correlation between Turbidimetric and Nephelometric Methods of Measuring C-Reactive Protein in Patients with Unstable Angina or Non-ST Elevation Acute Myocardial Infarction. *Arq Bras Cardiol* **2003**, *81* (2), 133-136.

11. Fakanya, W. M.; Tothill, I. E., Detection of the Inflammation Biomarker C-Reactive Protein in Serum Samples: Towards an Optimal Biosensor Formula. *Biosensors (Basel)* **2014**, *4* (4), 340-57.

12. Xu, J. P.; Ji, J.; Chen, W. D.; Shen, J. C., Novel Biomimetic Polymersomes as Polymer Therapeutics for Drug Delivery. *J Control Release* **2005**, *107* (3), 502-12.

13. Matsuno, R.; Ishihara, K., Integrated Functional Nanocolloids Covered with Artificial Cell Membranes for Biomedical Applications. *Nano Today* **2011**, *6* (1), 61-74.

14. Ahmed, M.; Jawanda, M.; Ishihara, K.; Narain, R., Impact of the Nature, Size and Chain Topologies of Carbohydrate-Phosphorylcholine Polymeric Gene Delivery Systems. *Biomaterials* **2012**, *33* (31), 7858-70.

15. Wang, Q.; Jin, H.; Xia, D.; Shao, H.; Peng, K.; Liu, X.; Huang, H.; Zhang, Q.; Guo, J.; Wang, Y.; Crommen, J.; Gan, N.; Jiang, Z., Biomimetic Polymer-Based Method for Selective Capture of C-Reactive Protein in Biological Fluids. *ACS Appl Mater Interfaces* **2018**, *10* (49), 41999-42008.

16. Kitayama, Y.; Takeuchi, T., Localized Surface Plasmon Resonance Nanosensing of C-Reactive Protein with Poly(2-Methacryloyloxyethyl Phosphorylcholine)-Grafted Gold Nanoparticles Prepared by Surface-Initiated Atom Transfer Radical Polymerization. *Anal Chem* **2014**, *86* (11), 5587-94.

17. Yoshimoto, J.; Sangsuwan, A.; Osaka, I.; Yamashita, K.; Iwasaki, Y.; Inada, M.; Arakawa, R.; Kawasaki, H., Optical Properties of 2-Methacryloyloxyethyl Phosphorylcholine-Protected Au₄Nanoclusters and Their Fluorescence Sensing of C-Reactive Protein. *J Phys Chem C* **2015**, *119* (25), 14319-14325.

18. Park, J.; Kurosawa, S.; Watanabe, J.; Ishihara, K., Evaluation of 2-Methacryloyloxyethyl Phosphorylcholine Polymeric Nanoparticle for Immunoassay of C-Reactive Protein Detection. *Anal Chem* **2004**, *76* (9), 2649-2655.

19. Iwasaki, Y.; Kimura, T.; Orisaka, M.; Kawasaki, H.; Goda, T.; Yusa, S., Label-Free Detection of C-Reactive Protein Using Highly Dispersible Gold Nanoparticles Synthesized by Reducible Biomimetic Block Copolymers. *Chem Commun (Camb)* **2014**, *50* (42), 5656-8.
20. Pinyorosphatum, C.; Chaiyo, S.; Sae-Ung, P.; Hoven, V. P.; Damsongsang, P.; Siangproh, W.; Chailapakul, O., Disposable Paper-Based Electrochemical Sensor Using Thiol-Terminated Poly(2-Methacryloyloxyethyl Phosphorylcholine) for the Label-Free Detection of C-Reactive Protein. *Mikrochim Acta* **2019**, *186* (7), 472.
21. Gu, H.; Xu, K.; Xu, C.; Xu, B., Biofunctional Magnetic Nanoparticles for Protein Separation and Pathogen Detection. *Chem Commun (Camb)* **2006**, (9).
22. Tsai HY, H. C., Chiu IW, Fuh CB. , Detection of C-Reactive Protein Based on Immunoassay Using Antibody-Conjugated Magnetic Nanoparticles. *Anal Chem* **2007**, *79* (21), 8416-8419.
23. Zhu, X.; Duan, D.; Publicover, N. G., Magnetic Bead Based Assay for C-Reactive Protein Using Quantum-Dot Fluorescence Labeling and Immunoaffinity Separation. *Analyst* **2010**, *135* (2), 381-9.
24. Yang, S. F.; Gao, B. Z.; Tsai, H. Y.; Fuh, C. B., Detection of C-Reactive Protein Based on a Magnetic Immunoassay by Using Functional Magnetic and Fluorescent Nanoparticles in Microplates. *Analyst* **2014**, *139* (21), 5576-81.
25. Kim, E.; Lee, S. G.; Kim, H.-C.; Lee, S. J.; Baek, C. S.; Choi, E.-S.; Jeong, S. W., Phosphocholine-Modified Magnetic Nanoparticles for Isolation of C-Reactive Protein from Human Serum. *Separ Sci Tech* **2013**, *48* (17), 2600-2607.
26. Iwasaki, S.; Kawasaki, H.; Iwasaki, Y., Label-Free Specific Detection and Collection of C-Reactive Protein Using Zwitterionic Phosphorylcholine-Polymer-Protected Magnetic Nanoparticles. *Langmuir* **2019**, *35* (5), 1749-1755.
27. Boonjamnian, S.; Trakulsujaritchook, T.; Srisook, K.; Hoven, V. P.; Nongkhai, P. N., Biocompatible Zwitterionic Copolymer-Stabilized Magnetite Nanoparticles: a Simple One-Pot Synthesis, Antifouling Properties and Biomagnetic Separation. *RSC Advances* **2018**, *8* (65), 37077-37084.
28. Adeoye, A. O. M.; Kayode, J. F.; Oladapo, B. I.; Afolabi, S. O., Experimental Analysis and Optimization of Synthesized Magnetic Nanoparticles Coated with PMAMPC-

MNPs for Bioengineering Application. *St. Petersburg Polytechnical University Journal: Physics and Mathematics* **2017**, *3* (4), 333-338.

29. Akkahat, P.; Kiatkamjornwong, S.; Yusa, S.; Hoven, V. P.; Iwasaki, Y., Development of a Novel Antifouling Platform for Biosensing Probe Immobilization from Methacryloyloxyethyl Phosphorylcholine-Containing Copolymer Brushes. *Langmuir* **2012**, *28* (13), 5872-81.

30. Khunsuk, P. O.; Chawalitpong, S.; Sawutdeechaikul, P.; Palaga, T.; Hoven, V. P., Gold Nanorods Stabilized by Biocompatible and Multifunctional Zwitterionic Copolymer for Synergistic Cancer Therapy. *Mol Pharm* **2018**, *15* (1), 164-174.

31. Wang, L.; Benicewicz, B. C., Synthesis and Characterization of Dye-Labeled Poly(methacrylic acid) Grafted Silica Nanoparticles. *ACS Macro Letters* **2013**, *2* (2), 173-176.

32. Goda, T.; Tabata, M.; Sanjoh, M.; Uchimura, M.; Iwasaki, Y.; Miyahara, Y., Thiolated 2-Methacryloyloxyethyl Phosphorylcholine for an Antifouling Biosensor Platform. *Chem Commun (Camb)* **2013**, *49* (77), 8683-5.

33. Chen, S. H.; Fukazawa, K.; Inoue, Y.; Ishihara, K., Photoinduced Surface Zwitterionization for Antifouling of Porous Polymer Substrates. *Langmuir* **2019**, *35* (5), 1312-1319.

34. Sae-Ung, P.; Kolewe, K. W.; Bai, Y.; Rice, E. W.; Schiffman, J. D.; Emrick, T.; Hoven, V. P., Antifouling Stripes Prepared from Clickable Zwitterionic Copolymers. *Langmuir* **2017**, *33* (28), 7028-7035.

35. Goto, Y.; Matsuno, R.; Konno, T.; Takai, M.; Ishihara, K., Polymer Nanoparticles Covered with Phosphorylcholine Groups and Immobilized with Antibody for High-Affinity Separation of Proteins. *Biomacromolecules* **2008**, *9*, 828-833.

36. Nishizawa, K.; Takai, M.; Ishihara, K., A Bioconjugated Phospholipid Polymer Biointerface with Nanometer-Scaled Structure for Highly Sensitive Immunoassays. *Methods Mol Biol* **2011**, *751*, 491-502.

37. Tajima, N.; Takai, M.; Ishihara, K., Significance of Antibody Orientation Unraveled: Well-Oriented Antibodies Recorded High Binding Affinity. *Anal Chem* **2011**, *83* (6), 1969-76.

38. Gao, L.; Wu, J.; Lyle, S.; Zehr, K.; Cao, L.; Gao, D., Magnetite

- Nanoparticle-linked Immunosorbent Assay. *J. Phys. Chem. C* **2008**, *112* (44), 17357-17361.
39. Zhuang, J.; Zhang, J.; Gao, L.; Zhang, Y.; Gu, N.; Feng, J.; Yang, D.; Yan, X., A Novel Application of Iron Oxide Nanoparticles for Detection of Hydrogen Peroxide in Acid Rain. *Mater Lett* **2008**, *62* (24), 3972-3974.
40. Zhang, Z.; Wang, Z.; Wang, X.; Yang, X., Magnetic Nanoparticle-Linked Colorimetric Aptasensor for the Detection of Thrombin. *Sens Actuator B-Chem* **2010**, *147* (2), 428-433.
41. Liu, Y.; Yuan, M.; Qiao, L.; Guo, R., An Efficient Colorimetric Biosensor for Glucose Based on Peroxidase-Like Protein-Fe₃O₄ and Glucose Oxidase Nanocomposites. *Biosens Bioelectron* **2014**, *52*, 391-6.
42. Gao, L.; Zhuang, J.; Nie, L.; Zhang, J.; Zhang, Y.; Gu, N.; Wang, T.; Feng, J.; Yang, D.; Perrett, S.; Yan, X., Intrinsic Peroxidase-Like Activity of Ferromagnetic Nanoparticles. *Nat Nanotechnol* **2007**, *2* (9), 577-83.
43. Huang, X.; Nan, Z., Porous 2D FeS₂ Nanosheets as a Peroxidase Mimic for Rapid Determination of H₂O₂. *Talanta* **2020**, *216*, 120995.
44. Woo, M. A.; Kim, M. I.; Jung, J. H.; Park, K. S.; Seo, T. S.; Park, H. G., A Novel Colorimetric Immunoassay Utilizing the Peroxidase Mimicking Activity of Magnetic Nanoparticles. *Int J Mol Sci* **2013**, *14* (5), 9999-10014.
45. Liu, Q.; Li, H.; Zhao, Q.; Zhu, R.; Yang, Y.; Jia, Q.; Bian, B.; Zhuo, L., Glucose-Sensitive Colorimetric Sensor Based on Peroxidase Mimics Activity of Porphyrin-Fe₃O₄ Nanocomposites. *Mater Sci Eng C Mater Biol Appl* **2014**, *41*, 142-51.
46. Pan, Y.; Li, N.; Mu, J.; Zhou, R.; Xu, Y.; Cui, D.; Wang, Y.; Zhao, M., Biogenic Magnetic Nanoparticles from Burkholderia Sp. YN01 Exhibiting Intrinsic Peroxidase-Like Activity and their Applications. *Appl Microbiol Biotechnol* **2015**, *99* (2), 703-15.
47. Park, J. Y.; Jeong, H. Y.; Kim, M. I.; Park, T. J., Colorimetric Detection System for Salmonella Typhimurium Based on Peroxidase-Like Activity of Magnetic Nanoparticles with DNA Aptamers. *J Nanomater* **2015**, *2015*, 1-9.
48. Zhang, L.; Huang, R.; Liu, W.; Liu, H.; Zhou, X.; Xing, D., Rapid and Visual Detection of Listeria Monocytogenes Based on Nanoparticle Cluster Catalyzed Signal Amplification. *Biosens Bioelectron* **2016**, *86*, 1-7.

49. Thanyasrisung, P.; Vittayaprasit, A.; Matangkasombut, O.; Sugai, M.; Na Nongkai, P.; Saipia, S.; Hoven, V. P., Separation and Detection of Mutans Streptococci by Using Magnetic Nanoparticles Stabilized with a Cell Wall Binding Domain-Conjugated Polymer. *Anal Methods* **2018**, *10* (27), 3332-3339.
50. Wei, Y.; Han, B.; Hu, X.; Lin, Y.; Wang, X.; Deng, X., Synthesis of Fe₃O₄ Nanoparticles and their Magnetic Properties. *Procedia Eng* **2012**, *27*, 632-637.
51. Jiang, W.; Wu, Y.; He, B.; Zeng, X.; Lai, K.; Gu, Z., Effect of Sodium Oleate as a Buffer on the Synthesis of Superparamagnetic Magnetite Colloids. *J Colloid Interface Sci* **2010**, *347* (1), 1-7.
52. Vilela, C.; Moreirinha, C.; Almeida, A.; Silvestre, A. J. D.; Freire, C. S. R., Zwitterionic Nanocellulose-Based Membranes for Organic Dye Removal. *Materials (Basel)* **2019**, *12* (9).
53. Kassel, M.; Gerke, J.; Ley, A.; Vana, P., Surface Modification of Wood Flour via ARGET ATRP and Its Application as Filler in Thermoplastics. *Polymers (Basel)* **2018**, *10* (4).
54. Potempa, L. A.; Yao, Z. Y.; Ji, S. R.; Filep, J. G.; Wu, Y., Solubilization and Purification of Recombinant Modified C-Reactive Protein from Inclusion Bodies Using Reversible Anhydride Modification. *Biophys Rep* **2015**, *1*, 18-33.
55. Meyer, M. H.; Hartmann, M.; Krause, H. J.; Blankenstein, G.; Mueller-Chorus, B.; Oster, J.; Miethe, P.; Keusgen, M., CRP Determination Based on a Novel Magnetic Biosensor. *Biosens Bioelectron* **2007**, *22* (6), 973-9.
56. Deegan, O.; Walshe, K.; Kavanagh, K.; Doyle, S., Quantitative Detection of C-Reactive Protein Using Phosphocholine-Labelled Enzyme or Microspheres. *Anal. Biochem.* **2003**, *312* (2), 175-181.
57. Shiesh, S. C.; Chou, T. C.; Lin, X. Z.; Kao, P. C., Determination of C-Reactive Protein with an Ultra-Sensitivity Immunochemiluminometric Assay. *J Immunol Methods* **2006**, *311* (1-2), 87-95.
58. Chang, C. H.; Lai, Z. X.; Lin, H. L.; Yang, C. C.; Chen, H. H.; Yang, S. Y.; Horng, H. E.; Hong, C. Y.; Yang, H. C.; Lin, H. C., Use of Immunomagnetic Reduction for C-Reactive Protein Assay in Clinical Samples. *Int J Nanomedicine* **2012**, *7*, 4335-40.



จุฬาลงกรณ์มหาวิทยาลัย
CHULALONGKORN UNIVERSITY

VITA

NAME Ms. Suttawan Saipia

DATE OF BIRTH 26 July 1994

PLACE OF BIRTH Trang, Thailand

INSTITUTIONS ATTENDED Bachelor degree from Department of Chemistry, Faculty of Science, Chulalongkorn University, Bangkok in 2016.

HOME ADDRESS 73 Moo 4 Na Wong Subdistrict, Huai Yot District, Trang Province 92210

PUBLICATION Proceeding: 23 July 2020, Poster presentation in Biomedical, Smart and Conductive Materials (PETROMAT 2020), Bangkok Thailand